1984

The electrochemical dissolution of copper sulfides using a fluidized bed electrochemical reactor

David Lloyd Felker
Iowa State University

Felker, David Lloyd

THE ELECTROCHEMICAL DISSOLUTION OF COPPER SULFIDES USING A FLUIDIZED BED ELECTROCHEMICAL REACTOR

Iowa State University PH.D. 1984

PLEASE NOTE:

In all cases this material has been filmed in the best possible way from the available copy. Problems encountered with this document have been identified here with a check mark __✓__.

1. Glossy photographs or pages _____
2. Colored illustrations, paper or print _____
3. Photographs with dark background _____
4. Illustrations are poor copy _____
5. Pages with black marks, not original copy _____
6. Print shows through as there is text on both sides of page _____
7. Indistinct, broken or small print on several pages ✓
8. Print exceeds margin requirements _____
9. Tightly bound copy with print lost in spine _____
10. Computer printout pages with indistinct print _____
11. Page(s) _____ lacking when material received, and not available from school or author.
12. Page(s) _____ seem to be missing in numbering only as text follows.
13. Two pages numbered _____. Text follows.
14. Curling and wrinkled pages _____
15. Dissertation contains pages with print at a slant, filmed as received _____
16. Other _____

_____

_____

University
Microfilms
International

The electrochemical dissolution of copper sulfides using a fluidized bed electrochemical reactor

by

David Lloyd Felker

A Dissertation Submitted to the
Graduate Faculty in Partial Fulfillment of the
Requirements for the Degree of
DOCTOR OF PHILOSOPHY

Major: Chemical Engineering

Approved:

Signature was redacted for privacy.

In Charge of Major Work

Signature was redacted for privacy.

For the Major Department

Signature was redacted for privacy.

For the Graduate College

Iowa State University
Ames, Iowa

1984

TABLE OF CONTENTS

DEDICATION

To Edie.

LIST OF SYMBOLS AND ABBREVIATIONS

A_i = activity of reactant i

a_i = stoichiometric coefficient for reactant i

B_i = activity of product i

b_i = stoichiometric coefficient for product i

$C_{H^+}(r)$ = analytical concentration of H^+ at position r, moles/m^3

$C_{H^+}^{bulk}$ = bulk H^+ concentration, moles/m^3

$\bar{C}$ = dimensionless concentration

CE_j = current efficiency for reaction j, %

D_i = diffusion coefficient for species i, m^2/sec

E = electrode potential, V

E_j^o = standard electrode potential for reaction j, V

F = Faraday's constant, A s/equiv.

I = current, A

K_j = equilibrium constant for reaction j

N_k = moles of solid k

N_k^o = initial moles of solid k

n_j = electrons transferred for reaction j

R = ideal gas constant, Pa $mole^{-1}$ K^{-1}

R_o = initial radius of chalcopyrite particle, m

$\bar{R}$ = dimensionless radial position

r = radial position in product layer, m

T = absolute temperature, K

$\bar{T}$ = dimensionless time

t = time, s

$\bar{V}_k$ = molar volume for solid k, m^3/mole

$\nu_{j,i}$ = stoichiometric coefficient for species i in reaction j

λ = dimensionless constant

$\alpha_{c,j}$ = cathodic transfer coefficient for reaction j

$\alpha_{a,j}$ = anodic transfer coefficient for reaction j

ε = product layer porosity

γ_j = activity coefficient of j

Π = product over i species

I. INTRODUCTION

Chalcopyrite, $CuFeS_2$, is one of the most abundant copper bearing minerals in the U.S. Oxidative leaching, and smelting and refining, are the most common methods used for recovering copper from chalcopyrite. One of the problems associated with oxidative leaching is the formation of an elemental sulfur product layer around the unreacted chalcopyrite core. The sulfur coating slows the reaction by inhibiting both the diffusion of the oxidant to the unreacted core, and the diffusion of the copper and iron species to the bulk solution. Another problem with leaching is that the iron and copper are oxidized simultaneously. Both appear in the bulk solution in their most oxidized states. This means that the Fe (III) must be removed from solution before electrowinning the copper, otherwise the electrowinning current efficiency will be low due to the reduction of Fe (III) and the simultaneous dissolution of the copper by chemical reaction with Fe (III). One of the major problems with the smelting and refining of chalcopyrite is the production of environmentally hazardous sulfur dioxide gas.

The direct electrodissolution of copper sulfide ore slurries could reduce the number of steps involved in the copper recovery process, possibly leading to large energy and economic savings. The potential application of electrodissolution processes in hydrometallurgy has been reviewed by Bautista and Flett [3].

This dissertation is based on the investigation of a proposed two stage electrochemical dissolution process for separating the copper, iron

and sulfur from chalcopyrite. The study focused mainly on the electrochemical dissolution of chalcopyrite because it is the most complex, and generally considered to be the most difficult, of the copper sulfide ores to process. To a lesser extent, the electrochemical dissolution of digenite, $Cu_{1.8}S$; covellite, CuS; chalcocite, Cu_2S and iron pyrite, FeS_2 were studied.

The following description of the proposed electrodissolution process is by no means meant to be an exhaustive explanation of the process. It is merely meant as an overview for providing the reader with a general understanding of the process. Specifics dealing with the chemistry, thermodynamics, kinetics, etc. will be addressed in detail later.

Stage #1 : A fluidized bed of chalcopyrite particles was reduced to digenite in the cathode chamber of a fluidized bed electrochemical reactor (FBER).

$$1.8\ CuFeS_2 + 5.2\ H^+ + 1.6\ e^- \longrightarrow Cu_{1.8}S + 2.6\ H_2S + 1.8\ Fe^{2+} \quad (1)$$

Reaction (1) took place in an acidic electrolyte solution (liquid phase #1). The majority of the $Cu_{1.8}S$ adhered to the surface of the unreacted $CuFeS_2$, constituting the starting material for the second stage of the process. The Fe liberated during the reduction of $CuFeS_2$ dissolved in the electrolyte as Fe (II). No copper dissolved into solution, all remained in the solid phase. The sulfur from the reacted chalcopyrite formed 2 products; gaseous H_2S and $Cu_{1.8}S$. Seventy-two percent of the original S was removed with the gas phase as H_2S. Assuming that the $Cu_{1.8}S$ layer

occupied the volume vacated by the reacted $CuFeS_2$, then the solid phase product should have had a 67% void volume (based on the known molar volumes for $CuFeS_2$ and $Cu_{1.8}S$).

Stage #2 : The $Cu_{1.8}S$ product layer resulting from stage #1 was oxidized to dissolved copper and elemental sulfur. The dissolution took place in two steps. First, the $Cu_{1.8}S$ was oxidized to Cu (I) and CuS.

$$Cu_{1.8}S \longrightarrow CuS + 0.8\ Cu^{+} + 0.8\ e^{-} \qquad (2)$$

The CuS was then oxidized to Cu (II) and elemental sulfur, S^{o}.

$$CuS \longrightarrow Cu^{2+} + S^{o} + 2\ e^{-} \qquad (3)$$

Both reactions took place in the same acidic electrolyte solution (liquid phase #2). As a result of reaction (2), about 45% of the Cu contained in the $Cu_{1.8}S$ was dissolved in the liquid phase as Cu (I). The 26% decrease in molar volume from $Cu_{1.8}S$ to CuS ensured that a porous product layer was produced during reaction (2). All of the CuS product resulting from reaction (2) adhered to the unreacted $Cu_{1.8}S$ and $CuFeS_2$. Formation of slimes was not a problem.

The CuS product from reaction (2) was oxidized to Cu (II) and elemental sulfur according to reaction (3). The amorphous sulfur layer coated the unreacted CuS and $CuFeS_2$. The coating was relatively porous due to the 19% decrease in molar volume from CuS to S.

A third stage would be used in a commercial copper recovery operation; the recovery of the dissolved copper as cathodic copper.

$$Cu^{+} + e^{-} \longrightarrow Cu^{o} \qquad (4)$$

$$Cu^{2+} + 2\,e^{-} \longrightarrow Cu^{o} \qquad (5)$$

However, this portion of the metal recovery process was not investigated in this study.

In summary, the net reaction resulting from the addition of reactions (1), (2), (3) and (4) was:

$$1.8\ CuFeS_2 + 5.2\ H^{+} \xrightarrow{(2.8\ e-)} Cu^{o} + 0.8\ Cu^{2+} + 1.8\ Fe^{2+} + 2.6\ H_2S + S^{o} \qquad (6)$$

The proposed electrochemical dissolution process represents a method for separating the copper, iron, and sulfur from chalcopyrite by a series of reduction and oxidation reactions. The only reagents consumed are hydrogen ions and electrons. The final products of the process include an iron-rich solution (liquid phase #1), a copper-rich solution (liquid phase #2), elemental sulfur and gaseous H_2S.

The general goal of the research reported in this dissertation was to investigate the feasibility of the above described electrochemical dissolution/separation process for the recovery of copper from its sulfide ores using a fluidized bed electrochemical reactor. The results contained

in this dissertation indicate that the electrochemical dissolution process shows promise as a viable route for the electrohydrometallurgical processing of chalcopyrite, via digenite and covellite intermediates.

II. LITERATURE REVIEW

A. Mineral Dissolution

The electrochemical dissolution of chalcopyrite, digenite, chalcocite and covellite have been previously investigated. However, the idea of reacting chalcopyrite in stages, using one product as the next reactant and separating the iron and copper by electrochemically dissolving them in different electrolyte solutions, has never been reported in the literature.

1. Reduction of chalcopyrite

The intention of most researchers who studied the reduction of chalcopyrite was to upgrade the sulfide ore concentrate by reducing the iron and sulfur content. Biegler and Constable [6] investigated the reduction of chalcopyrite concentrate using a slurry electrode and found that the solid reduction products ranged in composition from digenite to chalcocite, with a small amount of elemental copper being formed by the following reaction.

$$Cu_2S + 2\,H^+ + 2\,e^- \longrightarrow 2\,Cu + 2\,H_2S \qquad (7)$$

Elemental copper production during the reduction of chalcopyrite to digenite would be an undesirable side reaction, because it would add to the number of electrons needed for the overall process outlined by

reaction (6). For the chalcopyrite that was reduced to elemental copper, reaction
(6) would have to be rewritten in order to balance the number of oxidation and reduction electrons.

$$1.8\ CuFeS_2 + 7.2\ H^+ \xrightarrow{(3.6\ e^-)} 1.8\ Cu^{2+} + 3.6\ H_2S + 1.8\ Fe^{2+} \qquad (8)$$

Comparing reaction (8) to (6); reaction (8) produces no elemental sulfur or elemental copper and requires 2 more H^+ than reaction (6). Reaction (6) is a 2.8 electron process while reaction (8) is a 3.6 electron processes.

During the electroreduction of chalcopyrite, H_2S gas is evolved and Fe^{2+} dissolved into the catholyte. The optimum operating conditions using a slurry electrolysis cell were reported by Biegler and Constable [6] and included using a 5M HCl electrolyte at a temperature of 80-90 ^oC with a solid cathode current density of about 1 A cm^{-2}. These conditions resulted in coulombic efficiencies in the 50-70% range for up to 95% chalcopyrite conversion.

In a study done by Biegler and Swift [8], solid electrodes of chalcopyrite (approximately 1 x 1 x 1.5 cm) were reduced in 2M H_2SO_4 at 20^oC. It was found that below about 10 mA cm^{-2} the product was mainly chalcocite with a small amount of djurleite, $Cu_{1.97}S$. Above 50 mA cm^{-2} the major product was found to be finely divided elemental copper. Biegler and Swift [8] calculated the standard reduction potentials for the formation of Cu_2S and $Cu_{1.97}S$ to be -0.138 V and -0.144 V, respectively.

Since these reduction potentials are so close to each other, it would be likely that when one mineral was formed the conditions would be favorable for the formation of the other.

Biegler and Swift [8] investigated the effect that the electrolyte composition and temperature had on the current efficiency for the reduction of chalcopyrite at 10 mA cm^{-2}. They found that below 0.6 M and above 2 M H_2SO_4, the overall current efficiency decreased. Using 2 M H_2SO_4 at 20°C, the current efficiency rapidly declined with time to 25%, while at 45 and 70°C it was usually greater than 75%. Using 6 M HCl and a current density of 10 mA cm^{-2}, the current efficiency at 20°C was usually greater than 75%. Using 1 M $HClO_4$ and a current density of 10 mA cm^{-2} at 25°C the current efficiency was reported to be greater than 90%. The authors found that for constant current experiments, the current efficiency generally decreased with time. They suggested that since the electrode potential remained within a few millivolts of the original value during the reduction reaction, that the decrease in current efficiency was due to the precipitation of nonconductive Fe (II) salts in the porous Cu_2S product layer.

One reason for reducing chalcopyrite to chalcocite is that chalcocite is easier to leach. Biegler and Constable [7] proposed a scheme for converting chalcopyrite to chalcocite prior to leaching. The reduction of chalcopyrite was carried out using a recirculating slurry electrolysis cell. Using a 4 M HCl electrolyte with a cathode current density of 830 mA cm^{-2} and 10^5 coulombs total current passed, the coulombic efficiency approached 60% at high particle recirculation rates. The authors' scheme

included subjecting the reacted $CuFeS_2$ to a $CuCl_2$ leach step to remove the Cu_2S product layer. They proposed using froth flotation to recover the remaining chalcopyrite before it was recirculated to the slurry electrolysis cell.

2. Oxidation of chalcopyrite

There has been a lot of interest in the exhaustive oxidative electrodissolution of chalcopyrite to Cu^{2+}, Fe^{3+} and S^o [4,10,30,33,41, 44,48,53,56]

$$CuFeS_2 \longrightarrow Cu^{2+} + Fe^{3+} + S^o + 5\ e^- \qquad (9)$$

There are 2 reasons for all the interest in the oxidation route: (a) it provides the shortest and simplest path for recovering copper from its sulfide ore concentrates and (b) the production of SO_2 is completely eliminated since the sulfur is recovered in the elemental form. The process is not without drawbacks though, i.e., the low current efficiency with respect to the production of Cu (II) and the production of Fe (III). The copper electrowinning stage would be less efficient if an extraction step were not used to remove the Fe (III) first.

Biegler and Swift [10] studied the electrochemistry of the anodic dissolution of $CuFeS_2$ in 1 M H_2SO_4 and in 1 M HCl by performing linear sweep voltammetry and potentiostatic electrolysis experiments. The experimental results indicated that $CuFeS_2$ was anodically more reactive in H_2SO_4 than in HCl. The current-voltage behavior resulting from the linear

sweep voltammetry experiments using 1 M H_2SO_4 and a rotating electrode indicated that above 1.1 V the current-voltage relationship was linear, reaching a maximum current of about 1.1 A m^{-2} at about 2.0 V. For 1 M HCl, the current increased to a maximum value of 2.6 A m^{-2} at about 2.5 V. During potentiostatic experiments, the physical properties of the sulfur product layer depended on the electrolyte composition and the electrode potential. At 1.0-1.1 V in 1 M H_2SO_4 and 1.1-1.2 V in 1 M HCl, the sulfur layer was reported to be black and toffee-like in consistency. Using 1 M HCl, an adherent, yellow, amorphous sulfur layer formed above 1.2 V. Under the same conditions, except using 1 M H_2SO_4 instead of 1 M HCl, the sulfur layer was nonadherent. Biegler and Swift [10] found the source of the mineral had little effect on the reactivity of the specimen.

Price and Chilton [48] studied the anodic dissolution of chalcopyrite and bornite, Cu_5FeS_4. They found that for both chalcopyrite and bornite, the conditions for maximum current and energy efficiencies included operating above 60°C and using a chloride-containing electrolyte. In sulfuric acid solutions, oxygen evolution became a problem after a short period of electrodissolution. The authors attributed this to the onset of Cu^{2+} diffusion control.

In a later publication by Price and Chilton [49], it was reported that during the anodic oxidation of bornite, a copper deficient intermediate forms; $Cu_{2.5}FeS_4$. Price and Chilton also reported that below 50°C the anodic dissolution of bornite was controlled by the solid state diffusion of Cu^+ to the electrode surface. Above 65°C, the dissolution was chemical reaction controlled.

Copper exists as Cu (I) in the chalcopyrite lattice, iron as Fe (III) and sulfur as S (II). Vargas and Inman [53] studied the anodic dissolution of chalcopyrite in sulfuric acid-sodium chloride solutions containing acetonitrile. They attempted to recover the copper in the Cu (I) form but reported finding only Cu (II). The idea of recovering copper as Cu(I) is very appealing since the energy savings during the electrowinning step would be considerable.

Various studies have been done on the electrodissolution of copper matte [42,54,55]. Recently Mehendale, Venkatachalam, and Mallikarjunan [42], studying the anodic dissolution of copper matte, found that copper dissolved preferentially to iron between the anodic potentials of 0.35-0.5 V vs. SCE. They attributed the observation to the selective oxidation of digenite and bornite over chalcopyrite (all phases being present in the copper matte). They also found that above 0.5 V vs. SCE, iron was dissolved along with the copper. Using the G^{o} values for the anodic dissolution of digenite, bornite and chalcopyrite, the authors calculated the E^{o} values vs. SHE to be 0.566 V, 0.505 V and 0.506 V for digenite, bornite and chalcopyrite, respectively. Their calculations would indicate that bornite and chalcopyrite should dissolve before digenite, contrary to their experimental findings.

3. Reduction of chalcocite

There have been no reports in the literature of attempts to quantitatively reduce chalcocite by electrochemical methods. However, there have been reports of the electrochemical reduction of chalcocite to

elemental copper occurring as a side reaction during the electroreduction of chalcopyrite [6,7,8]. Biegler and Swift [8] reported that elemental copper was formed at about -0.4 V vs NHE.

4. Oxidation of chalcocite

The electrooxidation of chalcocite has been a popular subject in the literature in recent years: [9,12,13,25,29,31,34,38,42,47,54,55]. The idea is not new however. Marchese [40] patented the idea in 1882. Attempts to commercialize the process were not successful due to the excessive cell voltage, electrode disintegration and poor cathode copper quality.

There were no reports in the literature that dealt specifically with the oxidation of digenite. However, it was reported as an intermediate oxidation product by Habashi and Torres-Acuna [29], who studied the anodic dissolution of Cu_2S along with the simultaneous deposition of copper. The authors reported the mechanism for the electrooxidative dissolution of Cu_2S in sulfate solutions to be as follows. The entire surface of the anode first reacts to form digenite.

$$Cu_2S \longrightarrow Cu_{1.8}S + 0.2\ Cu^+ + 2\ e^- \qquad (10)$$

During the first stage, no visible slimes are formed and the electrode changes from shiny gray to dark blue. A sharp rise in the electrode potential then occurs and the digenite is converted to covellite.

$$5\ Cu_{1.8}S \longrightarrow 4\ CuS + 5\ Cu^{+} + S + 5\ e^{-} \qquad (11)$$

Superimposed with the decomposition of digenite is the decomposition of covellite.

$$CuS \longrightarrow Cu^{2+} + S + 2\ e^{-} \qquad (12)$$

Although Habashi and Torres-Acuna proposed that the dissolution of chalcocite and digenite should yield Cu (I), they did not report finding any Cu (I). The absence of Cu (I) would be expected, since it is not stable in a SO_4^{2-} environment.

Etienne [17] postulated that the limiting step which causes the sharp rise in electrode potential during the dissolution of chalcocite (same phenomenon as described by Habashi and Torres-Acuna [29]) is the mass transfer limited transport of the Cu^{2+} ions out of the porous CuS product layer.

Hojo and Peters [34] performed a detailed study on the direct electrorefining of chalcocite, i.e., the simultaneous dissolution of Cu_2S and deposition of Cu^{2+}. Following the mechanism postulated by Etienne [17], Hojo and Peters calculated the product layer thickness at the time of potential increase to be approximately 1 mm. Using particles that were less than 2 mm in diameter, Hojo and Peters found that 30-45% of the copper was removed at essentially 100% current efficiency without a substantial increase in the anode potential.

Biegler and Swift [9] performed galvanostatic and voltammetric

experiments using chalcocite and digenite. They were attempting to clarify the anodic behavior of the minerals during electrooxidation. During the voltammetric experiments, it was found that a porous layer formed at low potentials causing the current to decrease greatly due to the reaction rate being limited by the rate of Cu^{2+} diffusion through the porous product layer. During galvanostatic experiments, the potential rose sharply at the onset of mass transfer limitation causing chalcocite to be oxidized directly to Cu(II) and elemental sulfur. The authors used a novel technique to obtain an in situ view of the movement of the product layer during electrolysis. The technique enabled them to observe the growth of the pores in the product layer and the movement of different colored bands, which were supposedly indicative of the changes in the chemical composition of the product layer. During the galvanostatic experiments, the sharp rise in electrode potential was accompanied by the appearance of a yellow product that was believed to be sulfur. The authors derived a model based on the diffusion of Cu^{2+} through the product layer which was qualitatively in agreement with the data. The model agreed with the observation that the time at which the increase in potential occurred was dependent on the quantity I^2t (I = current density, A cm^{-2} and t = transition time, s). The I^2t value was found to be constant during individual experiments and ranged from approximately 0.6 - 9.5 for chalcocite and 0.9 - 8.6 for digenite, depending on the electrolyte composition.

Mackinnon [38] performed experiments dealing with the anodic dissolution of chalcocite using a plane parallel FBER. It was reported

that an intermediate oxidation product, identified as blue-remaining covellite, $Cu_{1.1}S$, was the sole product formed using a 2 M H_2SO_4 electrolyte.

$$Cu_2S \longrightarrow Cu_{1.1}S + 0.9\ Cu^{2+} + 1.8\ e^- \qquad (13)$$

After all the Cu_2S had reacted to form $Cu_{1.1}S$, only O_2 evolution occurred. Addition of NaCl or KBr to the H_2SO_4 electrolyte prevented the generation of O_2 and resulted in approximately 95% copper extraction. The reaction of chalcocite was found to occur in 2 distinct stages. When using an acid sulfate solution, the first stage was the production of blue-remaining covellite. Upon addition the Cl^- or Br^- to the electrolyte, the $Cu_{1.1}S$ was oxidized to Cu^{2+} and S^o.

$$Cu_{1.1}S \longrightarrow 1.1\ Cu^{2+} + S^o + 2.2\ e^- \qquad (14)$$

The second stage, which required the presence of Cl^- or Br^-, had a substantial potential increase associated with it. Mackinnon suggested that part of the potential increase may have been due to the added resistance of the sulfur coating on the reacted particles.

Price [47] analyzed the published data on the electrooxidation of chalcocite by applying the principles of chronopotentiometry. Previous researchers [9,17,45] had argued that the sharp rise in electrode potential corresponded to the point at which the pores of the chalcocite/covellite product layer became saturated with nonconductive

copper salts. This forced the current to be supported by the formation of elemental sulfur at the outer product layer. Kuxmann and Biallass [36] and Brennet et al. [12] supported the idea that the oxidation of Cu_2S to CuS is not mass transfer limited by the diffusion of the copper salts to the bulk solution, but rather that it is limited by the solid state diffusion of the copper from the bulk to the surface of the reacting chalcocite. Price [47] concluded that the reaction mechanism was that of solid state diffusion. Reexamination of the previously reported data tends to support Price's conclusion. If the process were controlled by the diffusion of copper ions through the stagnant liquid in the porous product layer, one would expect to find a dependence of the diffusion limited current density on the bulk Cu (II) concentration. No such dependence was found by Biegler and Swift [9]. Furthermore, the formation of sulfur occurs after the potential rise, not before, indicating that the sulfur layer's formation is a result of the potential increase and not the cause of it [9]. Based on the analysis of the previously published data, Price [47] proposed a mechanism for the solid state diffusion controlled electrooxidation of Cu_2S (ionization states were ignored). At low electrode potential:

$$Cu_2S \longleftrightarrow Cu_{(2-X)}S + X\ Cu_{surf} \quad \text{(solid state diffusion)} \qquad (15)$$

$$Cu_{surf} \longrightarrow Cu^{2+} + 2\ e^- \quad \text{(electrooxidation)} \qquad (16)$$

At high electrode potential:

$$Cu_{(2-X)}S \longrightarrow (2-X)\ Cu^{2+} + S^{o} + 2(2-X)\ e^{-} \qquad (17)$$

Gerlach and Kuzeci [25] used carbon paste electroactive electrodes to study the oxidation of chalcocite. Their results agreed with the solid state diffusion control mechanism for the oxidation of chalcocite described by Price [47].

5. Reduction of covellite

There have been no reports in the literature dealing with the electroreduction of covellite to elemental copper.

6. Oxidation of covellite

Many researchers have reported that the electrodissolution of covellite occurs as an intermediate reaction during the dissolution of chalcocite (discussed above). However, there have only been a few reports in the open literature dealing specifically with the oxidation of covellite [4,26,32,39].

Mackinnon [39] studied the fluidized bed anodic dissolution of covellite. It was found that electrodissolution in a sulfuric acid electrolyte was accompanied by oxygen production. Addition of Cl^{-} or Br^{-} to the electrolyte prevented the production of O_2, even at large current density values. The results indicated that in halide ion containing electrolytes, the oxidation of covellite proceeds via an electron transfer mechanism involving the Cl_2/Cl^{-} or Br_2/Br^{-} redox reaction and the

covellite surface. Apparently, the kinetics of the reaction of O_2 with the covellite surface are unfavorable.

Ghali and Lewenstam [26] investigated the anodic electrodissolution of CuS in hydrochloric acid solutions. It was reported that the rate of dissolution was a function of the pH and the Cl^- concentration. Above 1 M Cl^-, CuS dissolution was reported to be accelerated by the formation of a $CuCl_2^-$ complex resulting from the chemical reaction of Cu^{2+} and CuS.

Bertram, Hillrichs and Muller [5] reported the successful dissolution of $CuFeS_2$ and Cu_2S in molten $ZnCl_2$-KCl. The current efficiency for both of the following reactions was reported to be nearly 100%.

$$CuFeS_2 \longrightarrow Cu^+ + Fe^{2+} + 2\ S^o + 3\ e^- \qquad (18)$$

$$Cu_2S \longrightarrow 2\ Cu^+ + 2\ S^o + 2\ e^- \qquad (19)$$

No passivation of the electrode surfaces was observed because the sulfur layer was liquified under the reaction conditions and floated to the top of the melt. The energy and economic implications of the process look very promising. The ability to dissolve the Cu in the Cu (I) state would cut the energy consumption by 50% for the Cu_2S process, and by 40% for the $CuFeS_2$ process.

7. Electrodissolution of pyrite

Peters and Majima [46] investigated the electrochemical reaction of pyrite in acid perchlorate solutions. The results of their experiments

indicated that pyrite could be cathodically dissolved below a potential of 0.62 V vs. NHE. The reaction products were Fe^{2+} and H_2S

$$FeS_2 + 4\,H^+ + 2\,e^- \longrightarrow Fe^{2+} + 2\,H_2S \qquad (20)$$

The current efficiency for reaction (20) was found to be very low; generally less than 35%. Hydrogen production was the main reaction.

The oxidation of pyrite was found to occur above 0.62 V vs. NHE; the products being Fe^{3+} and SO_4^{2-} [46]. Based on reaction (21), the current efficiency was nearly 100%. No elemental sulfur was detected.

$$FeS_2 + 8\,H_2O \longrightarrow Fe^{3+} + 2\,SO_4^{2-} + 16\,H^+ + 15\,e^- \qquad (21)$$

Biegler and Swift [11] reported that the anodic dissolution of FeS_2 produces both SO_4^{2-} (reaction (21)) and elemental sulfur (reaction (22)). Both reactions were found to occur in a variety of electrolytes including 1 M H_2SO_4, 1 M $HClO_4$ and 1 M HCl.

$$FeS_2 \longrightarrow Fe^{3+} + 2\,S^o + 3\,e^- \qquad (22)$$

B. Fluidized Bed Electrochemical Reactor

The fluidized bed electrochemical reactor (FBER) appeared in 1966 when Coeuret [15] and Fleischmann et al. [19] applied for patents almost simultaneously in France and Great Britain, respectively. Since then,

metal electrowinning cells, electrochemical dissolution reactors, electrochemical reactors for inorganic and organic synthesis, fuel cells and battery systems, and reactors for electro-initiated polymerization; all incorporating FBER technology, were investigated. A number of reviews concerned with the use of FBERs have been published [14,16,18,27,38,52].

There are basically two types of FBERs. Both configurations are depicted in Figure 1. The plane parallel electrode (PPE) is distinguished from the side-by-side electrode (SSE) in that the current and bulk electrolyte flows run parallel to each other in the PPE, and perpendicular in the SSE.

One of the characteristics that distinguishes a fluidized bed electrode from a solid planar electrode is that a solid electrode has a uniform potential over its entire surface. This is a result of the solid having essentially zero electrical resistance. A fluidized bed electrode has an electrical resistance associated with it. The resistance is a result of the fact that the individual particles are not all in contact with each other. Charge transfer to the particulate electrode only occurs when particles are in contact with the current feeder electrode.

Sabacky and Evans [50] reported that the metal phase conductivity of a copper particulate fluidized bed electrode was largely dependent on the bed expansion, and insignificantly dependent on particle size.

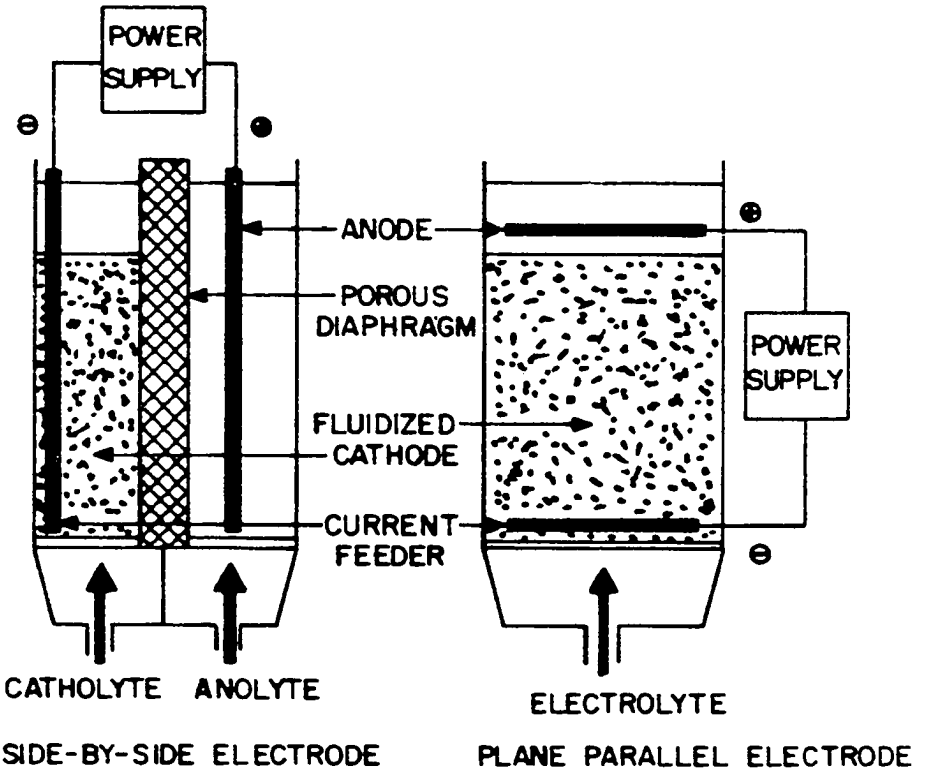

Figure 1. Schematic diagram of side-by-side and plane parallel fluidized bed electrochemical reactors

A number of mathematical models have been developed to describe the electrode potential distribution in a fluidized bed electrode. The pioneers in this area were Newman and Tobias [43], who developed the first mathematical model for describing the potential distribution in a porous electrode. Since then, a number of models have been developed. All have been based on the initial work done by Newman and Tobias. Sabacky and Evans [51] proposed a model for a FBER using a multicomponent electrolyte. Fleischmann et al. [20,21,22,23] and Goodridge et al. [28] incorporated the idea of particle charge sharing into their FBER models.

Experimental studies have also been done to establish the nature of the electrode potential as a function of electrode position, electrode geometry and operating conditions. Backhurst et al. [1] investigated the effect of increasing the fluidized bed width perpendicular or parallel to the direction of current flow. Bed expansion and particle size were also studied. Their results indicated that the total electrode current could be increased linearly with scale-up in the direction perpendicular to current flow. Scale-up parallel to the direction of current flow was reported to be limited to approximately one inch. Any increase above one inch resulted in very little, if any, increase in the electrode's current capacity.

Typical of the reports in the literature was one by Bareau and Coeuret [2], who measured the electrode potential over the length of a PPE used to anodically dissolve copper. The effects of static bed height, bed expansion and current density were examined. The results indicated that the fluidized bed electrode was almost inactive in the center portion of

the bed and that the top and bottom of the bed were very active. This phenomenon was confirmed by placing small copper wires throughout the bed and weighing them before and after an experiment.

III. EXPERIMENTAL PROGRAM

A. Materials and Equipment

A fluidized bed electrochemical reactor of the side-by-side type configuration, with separated anode and cathode chambers, was used for all the electrodissolution experiments. A schematic diagram of the reactor and the experimental set-up are shown in Figures 2 and 3. The electrode chambers of the FBER were separated by a porous Vycor glass diaphragm. The anolyte and catholyte solutions were circulated to and from separate reservoirs. The pores in the diaphragm were so small that no intermixing of the electrolytes occurred, other than the small amount due to diffusion through the pores. Essentially, the diaphragm was only porous enough to allow electrical contact between the solutions. The electrolytes were circulated through a constant temperature bath and their flow rates were controlled by separate pumps.

The outer chamber of the FBER was the working electrode chamber. The current feeder electrodes, which provided the electrical connection between the power supply and the fluidized bed electrode, extended from the top of the FBER down into the working electrode chamber. The feeder electrodes were made of pressed graphite powder.

Chalcopyrite from Messina, Transvaal, Republic of South Africa, chalcocite from Butte, Montana, and iron pyrite from Custer, South Dakota were used in the experiments. The minerals were all purchased from Ward's Scientific Establishment, Inc. The results of the chemical analysis of

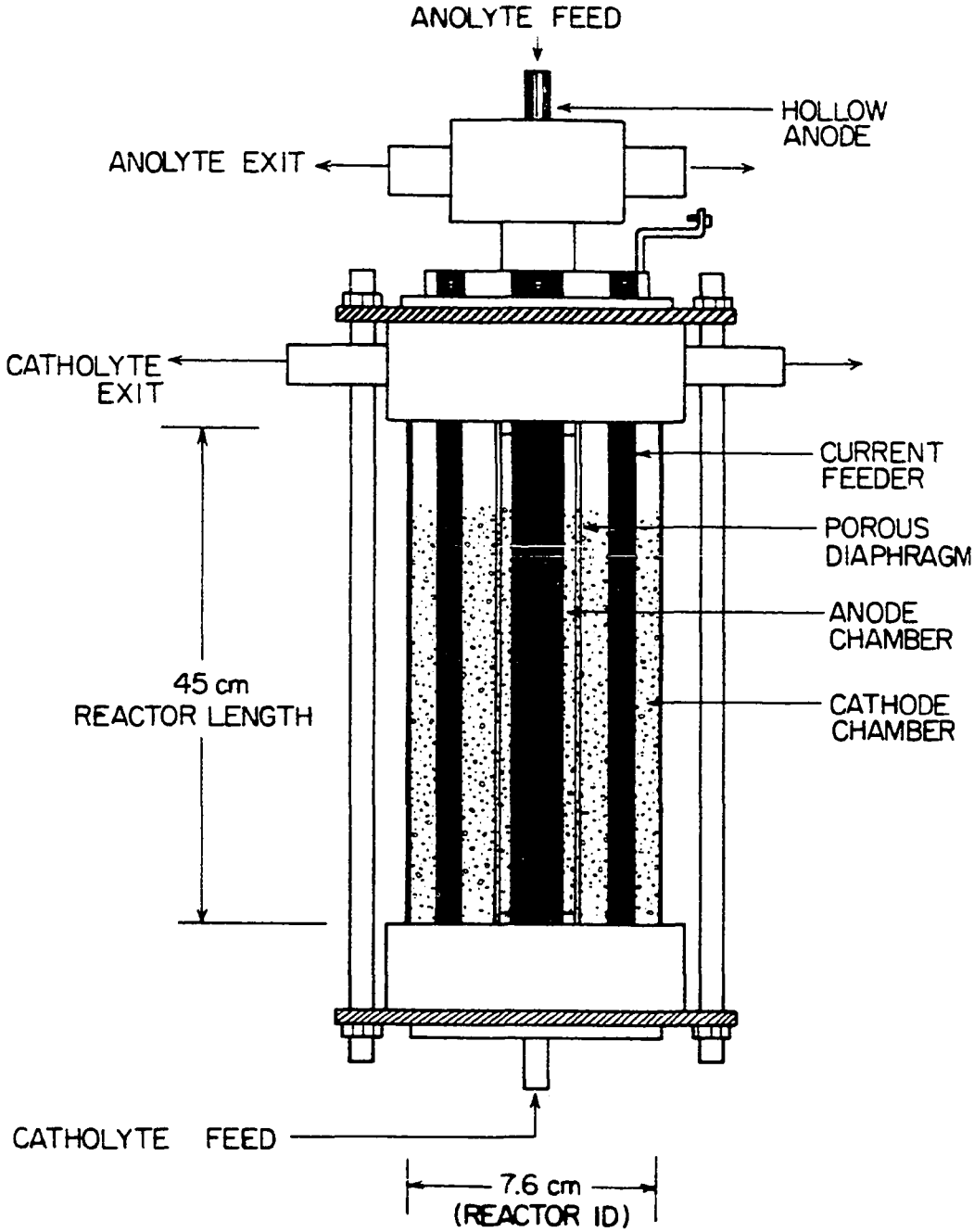

Figure 2. Diagram of the fluidized bed electrochemical reactor used in this study

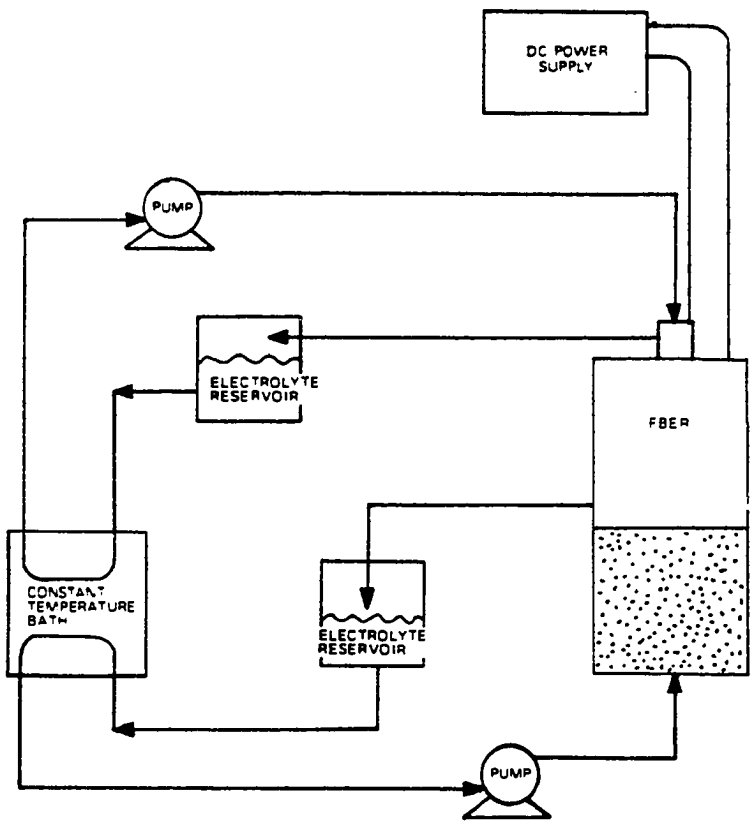

Figure 3. Diagram of the experimental apparatus used in this study

the chalcopyrite and chalcocite starting materials, presented in Table 1, indicate that the minerals were relatively pure. The minerals were crushed and screened into size fractions between 10 and 40 mesh. The particle size range used for individual experiments was only one or two screen sizes.

Analysis of the various reactants and products was accomplished using the following techniques: Atomic absorption spectophotometry was used to measure the total dissolved metal ion concentrations of copper and iron. Visible absorption spectrophotometry was used to determine the concentration of Cu (II) and Fe (III). X-ray powder diffraction crystallography, auger electron spectroscopy (AES), energy dispersion x-ray spectroscopy (EDXS), and chemical degradation were used to determine the composition of the different solid phases. A scanning electron microscope and an optical microscope were also used to examine the solid phases. A list of all of the major equipment, including the make and model, is given in the Appendix.

In order to minimize the chemical oxidation of the particles and/or electrolyte species by dissolved oxygen, all experiments were performed under an inert atmosphere of Ar or N_2.

B. Experimental Procedure

The range of operating conditions for the reduction-oxidation experiments are presented in Table 2. The first stage of the experiment was the reduction of chalcopyrite. The second stage involved the oxidation of the $Cu_{1.8}S$ product layer that was produced in stage 1. The

Table 1. Chemical analysis of chalcopyrite and chalcocite

Mineral	Origin	Element	Determined Mole %
$CuFeS_2$	Messina, Transvaal	Cu	24.7 ± 0.3 %
		Fe	25.0 ± 0.2 %
		S	47.7 ± 0.9 %
		Si	0.5 ± 0.1 %
Cu_2S	Butte, Montana	Cu	62.6 ± 0.3 %
		Fe	2.9 ± 0.4 %
		S	32.3 ± 0.9%
		Si	0.9 ± 0.1%

Table 2. Range of experimental conditions used in the present study

Reduction Experiment: Stage 1	
Initial catholyte volume:	10 l
Catholyte sample volume:	20 ml
Catholyte Acid Concentration:	4 M HCl, 4 M $HClO_4$, 2 M H_2SO_4 or 2.7 M H_3PO_4
Initial Fe (II) concentration:	0 M
Initial Cu (II) concentration:	0 M
Final Fe (II) concentration:	0.05–0.15 M
Final Cu (II) concentration:	0.0001–0.001 M
Catholyte flow rate:	15–60 ml sec^{-1}
Catholyte temperature:	15–58°C
Total cell current:	5–80 A
Initial mass $CuFeS_2$:	500 g
$CuFeS_2$ particle size:	0.250–2.0 mm
FBER static bed height:	2–6 cm
FBER bed width:	2.1 cm
FBER bed expansion:	5–20 %
Oxidation Experiment: Stage 2	
Initial anolyte volume:	10 l
Anolyte sample volume:	20 ml
Anolyte Acid Concentration:	4 M HCl, 4 M $HClO_4$, 2 M H_2SO_4 or 2.7 M H_3PO_4
Initial Fe (II) concentration:	0 M
Initial Cu (II) concentration:	0 M
Final Fe (II) concentration:	0.0001–0.05 M
Final Cu (II) concentration:	0.05–0.2 M
Anolyte flow rate:	15–60 ml sec^{-1}
Anolyte temperature:	15–58°C
Total cell current:	5–80 A
Initial mass $Cu_{1.8}S$:	20–100 g
FBER static bed height:	2–6 cm
FBER bed expansion:	0–20 %

following procedure was used to insure that the dissolved Fe species generated in stage 1 did not contaminate the electrolyte in stage 2: After stage 1 was completed, the electrolyte (liquid phase #1) was drained from the reactor and the particulate bed was washed with 2 liters of fresh electrolyte to remove any residual Fe metal ions. The flow lines of the system were also flushed with fresh electrolyte and the residual liquid was evacuated from the flow lines using compressed air. The new electrolyte (liquid phase #2) was then pumped into the reactor. The fluidized bed electrode's polarity was then reversed and the product from stage #1 was oxidized. It is important to realize that reaction (1) took place in a completely different electrolyte than that used for reactions (2) and (3). Thus, the Fe^{2+} produced by reaction (1) and the Cu^{2+} produced by reactions (2) and (3) were physically separated from each other.

C. Calculations

The experimental results were expressed using quantities such as the current efficiency, charge consumed and fractional current. The following section contains brief definitions of those quantities.

For an electrochemical reaction where reactant A is reduced to product B,

$$A + n\, e^- \longrightarrow b\, B \qquad (23)$$

Faraday's law relates the number of moles of B produced by a given quantity of electrical charge.

$$N = \frac{bIt}{nF} \tag{24}$$

where N = number of moles produced

b = stoichiometric coefficient for product B

I = current (amperes)

t = time of reaction (seconds)

n = number of electrons/mole of A reacting (equivalents/mole)

F = Faraday's constant (96,486 amp-sec/equivalent).

When a number of reactions occur simultaneously, it is common to write Faraday's law as

$$N_j = \frac{b_j I_j t}{n_j F} \tag{25}$$

where N_j = number of moles of product B_j produced

b_j = stoichiometric coefficient for product B_j

I_j = current supporting the reaction of A_j

t = time of reaction

n_j = number of electrons/mole of A_j reacting

The total electrical charge passed is equal to the sum of the charge consumed by the individual reactions.

$$(It)_{Total} = (It)_1 + (It)_2 + \ldots + (It)_j \tag{26}$$

Dividing the total charge by t, gives the total current used as a function of the sum of the individual currents supporting the j reactions.

$$I_{Total} = I_1 + I_2 + \ldots + I_j \tag{27}$$

Faraday's law (equation (25)) can be written in differential form as

$$\frac{dN_j}{dt} = \frac{b_j I_j}{n_j F} \tag{28}$$

Equation (28) indicates that the rate of change of the number of moles of component j with time will be proportional to the current supporting the reaction involving component j.

The current efficiency for a reaction is the fractional current supporting the particular reaction, expressed as a percentage.

$$CE_j = \frac{I_j}{I_{Total}} \times 100\% \tag{29}$$

IV. CHALCOPYRITE REDUCTION MODEL DEVELOPMENT

Eh-pH diagrams are based on equilibrium thermodynamics and therefore do not accurately describe the galvanically controlled reduction of chalcopyrite, which is a nonequilibrium process. Eh-pH diagrams do provide some help, though, in estimating what stable phases will form during chalcopyrite reduction. Figure 4 is an Eh-pH diagram for the system composed of Cu-Fe-S-O-H [24]. The predicted stable solid phases at a pH of zero and between an Eh of +0.35 and -0.6 are (in order of decreasing electrode potential): CuS, CuS and S^o, CuS, $Cu_{1.8}S$, Cu_2S, Cu_5FeS_4, $CuFeS_2$, Cu_5FeS_4, Cu_2S and Cu. The only stable dissolved species over the same Eh range, at pH = 0, is Fe^{2+}. The Eh-pH diagram predicts that dissolved Cu^{2+} is only stable above an Eh of approximately +0.35. The experimental work, upon which this dissertation is based, indicated that the stable phases formed during the reduction of chalcopyrite were similar to those predicted by equilibrium thermodynamics. However, kinetics has to be used to predict the rate of chalcopyrite reduction.

Figure 5 is a schematic diagram of a single reacting $CuFeS_2$ sphere. The dimensions and dissolved species concentrations referred to in the following model derivation are those shown in Figure 5. The physical description of the particle assumes that the $Cu_{1.8}S$ product layer occupies the volume left behind by the reacted $CuFeS_2$.

The porosity of the product layer can be estimated by assuming that the porosity of the product layer is due to the difference between the

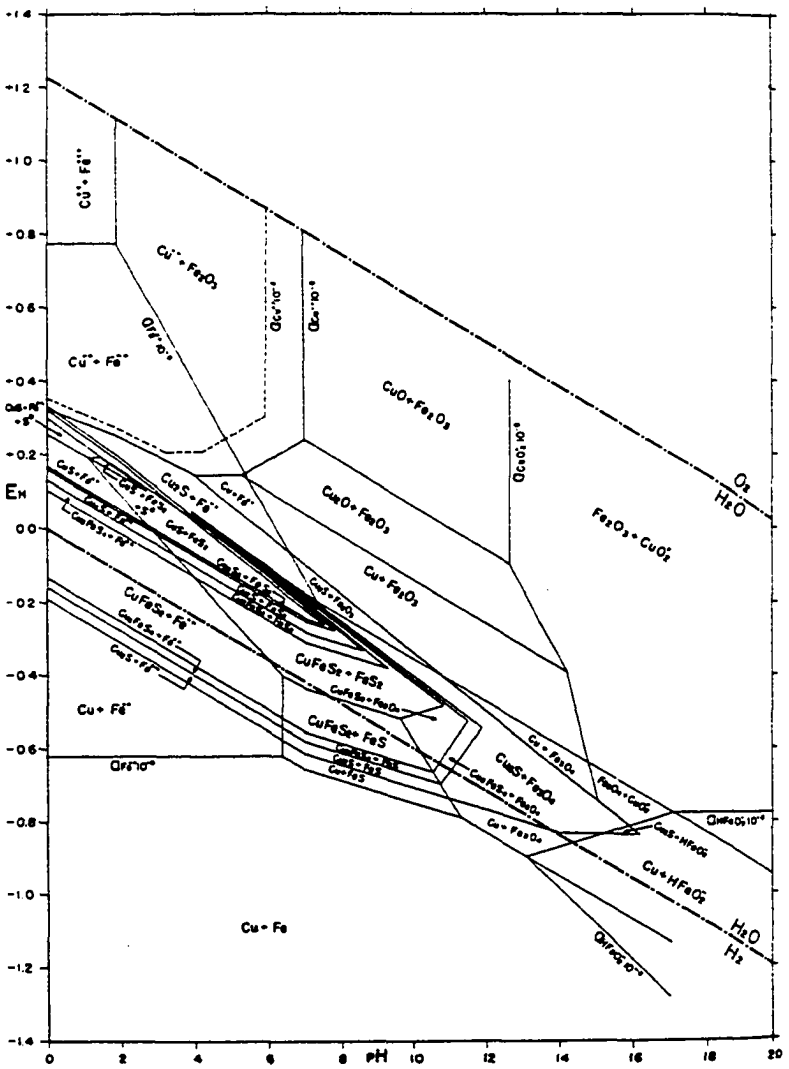

Figure 4. Eh-pH diagram for the system Cu-Fe-S-O-H at 25 °C, 1 atm and 10^{-4} m total sulfur

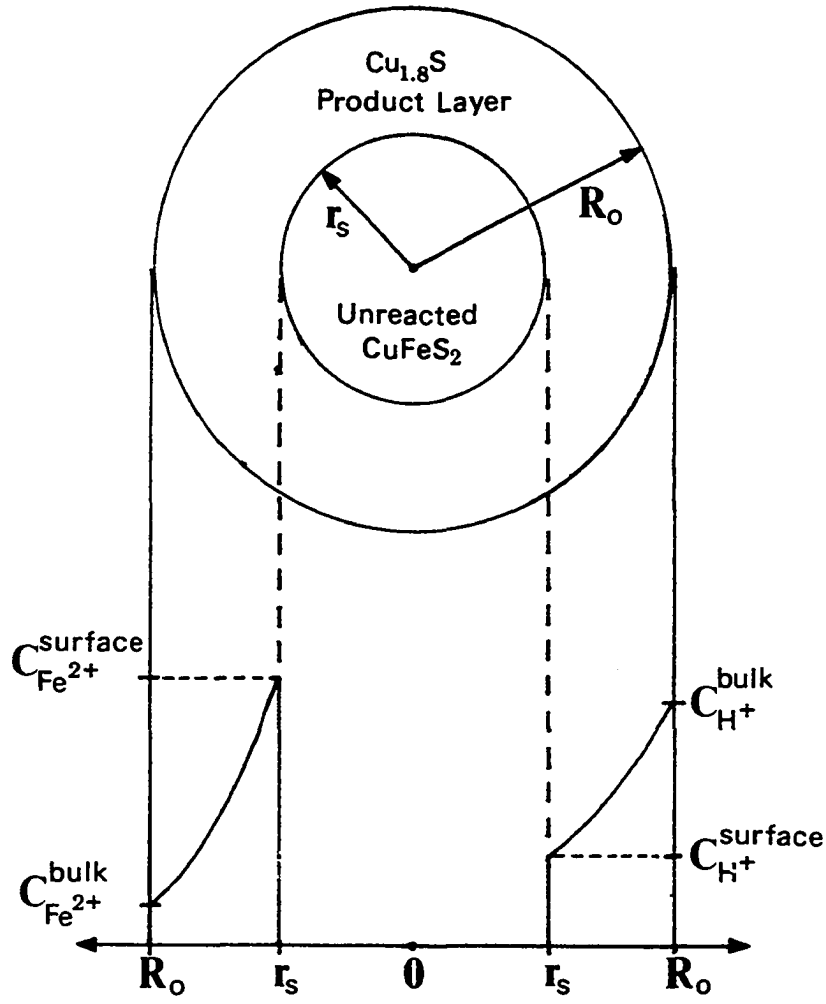

Figure 5. Schematic diagram of a single $CuFeS_2$ particle during electroreduction

molar volumes of $CuFeS_2$ and $Cu_{1.8}S$. The porosity is then

$$\varepsilon = 1 - \frac{\bar{V}_{Cu_{1.8}S}}{1.8\ \bar{V}_{CuFeS_2}} \qquad (30)$$

where $V_{Cu1.8S}$ = the molar volume of $Cu_{1.8}S$ = 26.0 cm^3/mole

V_{CuFeS2} = the molar volume of $CuFeS_2$ = 44.1 cm^3/mole

1.8 = the ratio of the stoichiometric coefficients relating the number of moles $CuFeS_2$ reacted per mole of $Cu_{1.8}S$ produced.

The physical reality of the situation might be different. The $Cu_{1.8}S$ product could collapse on the reacting surface, in which case the product layer would be less porous than expected. Or the $Cu_{1.8}S$ product could grow away from the reacting surface, in which case the product layer would be more porous than expected.

The fluid velocity in the FBER was large enough that the diffusional resistance of the hydrodynamic boundary layer was assumed to be negligible. Therefore, The concentrations at R_o in Figure 5 were chosen to be those of the bulk solution.

Heterogeneous electrochemical kinetics can be used to predict the electrochemical reaction rates for nonequilibrium systems, i.e., systems with a net cathodic or anodic current. The expression for the net current can be written in a form similar to the expression for a normal heterogeneous reaction. The net current is written as the sum of the

forward (cathodic) and reverse (anodic) currents.

$$I_{Net} = -nFAK\left[\Pi A_i^{a_i} \exp\left(\frac{-\alpha_c F(E-E^o)}{RT} \right) - \Pi B_i^{b_i} \exp\left(\frac{\alpha_a F(E-E^o)}{RT} \right) \right] \quad (31)$$

where A = the electrode surface area

F = Faraday's Constant

A_i = the activity of reactant i

a_i = the stoichiometric coefficient for A_i

B_i = the activity of product i

b_i = the stoichiometric coefficient for B_i

Π = the symbol specifying the product over i species

α_c = the transfer coefficient for the cathodic reaction

α_a = the transfer coefficient for the anodic reaction

E^o = the standard reduction potential

E = the electrode potential.

The rate of an electrochemical reaction is a function of the electrode potential. When the electrode is made cathodic, $E-E^o \S 0$, the cathodic term in equation (31) dominates and the equation for the net current becomes

$$I_{Net} = I_{Cathodic} = -nFAK\, \Pi A_i^{a_i} \exp\left(\frac{-\alpha_c F(E-E^o)}{RT} \right) \quad (32)$$

There were two reactions that occurred simultaneously during the cathodic reaction of chalcopyrite: The electrodissolution of $CuFeS_2$

according to reaction (33) and the evolution of H_2 according to reaction (34).

$$\nu_{1,CuFeS_2}\ CuFeS_2 + \nu_{1,H^+}\ H^+ + n_1\ e^- \longrightarrow \text{products} \qquad (33)$$

$$\nu_{2,H^+}\ H^+ + n_2\ e^- \longrightarrow \text{products} \qquad (34)$$

Reactions (33) and (34) have been written showing the reactants only. Specification of the product identities is not necessary in order to write the net current equations, provided of course that the anodic terms are negligible. By writing reactions (33) and (34) as above, it is assumed that only $CuFeS_2$ and H^+ are involved in the rate determining step for the reduction of $CuFeS_2$, and only H^+ is involved in the rate determining step for H_2 evolution.

Writing the cathodic currents for reactions (33) and (34) in the form of equation (32) gives

$$I_1 = -n_1 FAK_1\ a^q_{CuFeS_2}\ a^p_{H^+}\ \exp\left(\frac{-\alpha_{c,1}F(E-E_1^o)}{RT}\right) \qquad (35)$$

$$I_2 = -n_2 FAK_2\ a^s_{H^+}\ \exp\left(\frac{-\alpha_{c,2}F(E-E_2^o)}{RT}\right) \qquad (36)$$

where $q = \dfrac{\nu_{1,CuFeS_2}}{n_1}$ $\quad p = \dfrac{\nu_{1,H^+}}{n_1}$ $\quad s = \dfrac{\nu_{2,H^+}}{n_2}$

It must be stressed that no distinction has been made between the surface area terms in equations (35) and (36). It was assumed in writing equations (35) and (36) that both reactions take place on the same surface.

The sum of the current consumed by the individual reactions is equal to the total current, I_{Total}, consumed by the system. Assuming that only reactions (33) and (34) occur during the dissolution of $CuFeS_2$, the total current is given by

$$I_{Total} = -FA\left[n_1K_1\, a^{q}_{CuFeS_2}\, a^{p}_{H^+} \exp\left(\frac{-\alpha_{c,1}F(E-E^{o}_{1})}{RT}\right) + n_2K_2\, a^{s}_{H^+} \times \exp\left(\frac{-\alpha_{c,2}F(E-E^{o}_{2})}{RT}\right)\right] \quad (37)$$

Expressing the individual currents as a fraction of the total current gives

$$I_1 = \frac{I_{Total}\, n_1K_1\, a^{q}_{CuFeS_2}\, a^{p}_{H^+} \exp\left(\frac{\alpha_{c,1}F(E-E^{o}_{1})}{RT}\right)}{\left[n_1K_1\, a^{q}_{CuFeS_2}\, a^{p}_{H^+} \exp\left(\frac{\alpha_{c,1}F(E-E^{o}_{1})}{RT}\right) + n_2K_2\, a^{s}_{H^+} \exp\left(\frac{\alpha_{c,2}F(E-E^{o}_{2})}{RT}\right)\right]} \quad (38)$$

$$I_2 = \frac{I_{Total}\, n_2K_2\, a^{s}_{H^+} \exp\left(\frac{\alpha_{c,2}F(E-E^{o}_{2})}{RT}\right)}{\left[n_1K_1\, a^{q}_{CuFeS_2}\, a^{p}_{H^+} \exp\left(\frac{\alpha_{c,1}F(E-E^{o}_{1})}{RT}\right) + n_2K_2\, a^{s}_{H^+} \exp\left(\frac{\alpha_{c,2}F(E-E^{o}_{2})}{RT}\right)\right]} \quad (39)$$

The temperature dependence of equations (38) and (39) comes from the exponential terms. Temperature independence would then imply that

$$\alpha_{c,1}(E-E_1^o) = \alpha_{c,2}(E-E_2^o) \tag{40}$$

The fact that $CuFeS_2$ dissolution and H_2 evolution occur simultaneously and that there is no change in the rate of one reaction over the other when the temperature is increased, indicates that the activation energies for the reactions (33) and (34) are similar. (Experimental evidence for temperature independence is given in the results and discussion section of this dissertation.) It is therefore assumed that equation (40) is true and that the exponential terms in equations (38) and (39) cancel. The equations for I_1 and I_2 then simplify to the following equations.

$$I_1 = \frac{I_{Total}\ K'_{p-s}\ C_{H^+}^{p-s}}{(K'_{p-s}\ C_{H^+}^{p-s} + 1)} \tag{41}$$

$$I_2 = \frac{I_{Total}}{(K'_{p-s}\ C_{H^+}^{p-s} + 1)} \tag{42}$$

where

$$K'_{p-s} = \frac{n_1 K_1\ a_{CuFeS_2}^{q-s}\ \gamma_{H^+}^{p-s}}{n_2 K_2}$$

Mathematical expressions have now been derived which relate the individual currents to the total current and the H^+ concentration at the surface of the shrinking $CuFeS_2$ core. In order to mathematically model the cathodic dissolution of chalcopyrite, an equation must be derived that relates the fractional currents to the product layer thickness.

The reduction of chalcopyrite is assumed to be controlled by the concentration of H^+ at the reacting surface. The diffusion equation in spherical coordinates is used to describe the diffusion of H^+ from the bulk solution to the reacting surface.

$$\frac{d^2C_{H^+}(r)}{dr^2} + \frac{2}{r}\frac{dC_{H^+}(r)}{dr} = 0 \qquad (43)$$

The time derivative in the diffusion equation is neglected by invoking the pseudo steady state assumption.

Equation (43) contains no reaction term describing the consumption of H^+. The following boundary condition is used to describe the rate of H^+ consumption.

$$D_{H^+}\left.\frac{dC_{H^+}(r)}{dr}\right|_{r=r_s} = \frac{\frac{\nu_{1,H^+}}{n_1F} I_1 + \frac{\nu_{2,H^+}}{n_2F} I_2}{(4\pi r^2)\left(\frac{3\bar{V}_{CuFeS_2} N^o_{CuFeS_2}}{4\pi R_o^3}\right)} \qquad (44)$$

Equation (44) states that the flux of H^+ at the reacting surface is equal to the rate of consumption of H^+ by reactions (33) and (34). The

first term in the denominator on the right hand side of equation (44) describes the surface area of a single $CuFeS_2$ particle. The second term in the denominator describes the number of particles. The product of the two terms equals the total surface area of $CuFeS_2$. After substituting equations (41) and (42) for I_1 and I_2, equation (44) becomes

$$\frac{3\bar{V}_{CuFeS_2} N^{o}_{CuFeS_2} D_{H^+} r^2}{I_{Total} R_o^3} \frac{dC_{H^+}(r)}{dr} = \frac{\nu_{1,H^+} K'_{p-s} C^{p-s}_{H^+}(r)}{n_1 F(K'_{p-s} C^{p-s}_{H^+}(r) + 1)}$$

$$+ \frac{\nu_{2,H^+}}{n_2 F_2(K'_{p-s} C^{p-s}_{H^+}(r) + 1)} \qquad @ \quad r = r_s \qquad (45)$$

The other boundary condition used to solve equation (43) was the equation describing the H^+ concentration at the reacting $CuFeS_2$ surface as being equal to the bulk concentration of H^+.

$$C_{H^+}(r) = C^{bulk}_{H^+} \qquad @ \quad r = R_o \qquad (46)$$

The solution to the above boundary condition problem gives the H^+ concentration profile in the product layer.

$$C_{H^+}(r) = C^{bulk}_{H^+} \left[1 - \frac{1}{\lambda_1 \lambda_3} \left(\frac{\lambda_4 + \lambda_2}{\lambda_4 + 1} \right) \left(\frac{R_o}{r} - 1 \right) \right] \qquad (47)$$

where

$$\lambda_1 = \frac{3N^{o}_{CuFeS_2} \dfrac{n_1}{\nu_{1,CuFeS_2}} F D_{H^+}}{I_{Total} R_o^2}$$

$$\lambda_2 = \frac{n_1 \nu_{2,H^+}}{n_2 \nu_{1,H^+}}$$

$$\lambda_3 = \frac{\bar{V}_{CuFeS_2} C^{bulk}_{H^+} \nu_{1,CuFeS_2}}{\nu_{1,H^+}}$$

$$\lambda_4 = K'_{p-s} (C^{bulk}_{H^+})^{p-s}$$

The mass action equation for the reacting particle shown in Figure 5 gives the change in the moles of $CuFeS_2$ with time as a function of the current I_1.

$$\frac{dN_{CuFeS_2}}{dt} = \frac{\nu_{1,CuFeS_2} I_1}{n_1 F} \tag{48}$$

where N_{CuFeS2} = the total moles of $CuFeS_2$.

The mole fraction of $CuFeS_2$ reacted is related to the unreacted

particle radius by

$$\frac{N_{CuFeS_2}}{N^o_{CuFeS_2}} = \left(\frac{r_s}{R_o}\right)^3 \tag{49}$$

where N^o_{CuFeS2} = the number of moles of $CuFeS_2$ at t = 0.

Taking the derivative of equation (49) gives

$$\frac{dN_{CuFeS_2}}{dt} = \frac{3N^o_{CuFeS_2} r_s^2}{R_o^3} \frac{dr_s}{dt} \tag{50}$$

The relationship between the rate of change of r_s and the current supporting reaction (33) is obtained by combining equations (48) and (50).

$$\frac{3r_s^2}{R_o^3} \frac{dr_s}{dt} = \frac{\nu_{1,CuFeS_2} I_1}{n_1 F N^o_{CuFeS_2}} \tag{51}$$

Eliminating I_1 from equation (51) by substituting equation (41) for I_1 gives an equation representing the rate of change of the unreacted $CuFeS_2$ particle's radius to the H^+ concentration at the reaction surface.

$$\lambda_1\lambda_3 \bar{R}^2 \frac{d\bar{R}}{d\bar{T}} = \frac{\lambda_4 \bar{C}^{p-s} + \lambda_2}{\lambda_4 \bar{C}^{p-s} + 1} \tag{52}$$

where $\bar{R} = \frac{r}{R_o}$ $\quad \bar{C} = \frac{C_{H^+}(r)}{C^{bulk}_{H^+}}$ $\quad \bar{T} = \frac{I_{Total}\, t}{3N^o_{CuFeS_2} F}$

Substituting equation (47) into (52) gives the final equation that relates the rate of $CuFeS_2$ reduction to the radius of the unreacted $CuFeS_2$ particle.

$$\lambda_1\lambda_3 \bar{R}^2 \frac{d\bar{R}}{d\bar{T}} = \frac{\lambda_4 \left[1 - \frac{1}{\lambda_1\lambda_3} \left(\frac{\lambda_4 + \lambda_2}{\lambda_4 + 1} \right) \left(\frac{1}{\bar{R}} - 1 \right) \right]^{p-s} + \lambda_2}{\lambda_4 \left[1 - \frac{1}{\lambda_1\lambda_3} \left(\frac{\lambda_4 + \lambda_2}{\lambda_4 + 1} \right) \left(\frac{1}{\bar{R}} - 1 \right) \right]^{p-s} + 1} \qquad (53)$$

Integration of equation (53) between the limits of R=1 to R and T=0 to T gives the equation for the fraction of $CuFeS_2$ reacted versus time. An analytical solution can be obtained if p-s is an integer. Assuming that the stoichiometry of the rate determining reactions occurring during chalcopyrite reduction was that of reaction (1) and reaction (34) with $v_{2,H+} = 1$ and $n_2 = 1$, then p-s is 2.25. Equation (53), for the case of p-s = 2.25, was solved using a numerical integration program written for an Apple IIe computer.

V. RESULTS AND DISCUSSION

The major results of this work include (i) the derivation of a model that explains the results of the reduction of chalcopyrite over a wide variety of experimental conditions, (ii) elucidation of the conditions under which $Cu_{1.8}S$ and Cu_2S can be partially oxidized yielding dissolved Cu(I) and (iii) recommendations, based on experimental findings, for the conditions which lead to the most efficient separation and recovery of the Cu, Fe and S from chalcopyrite.

A. Electrochemistry Related to the Reduction of Chalcopyrite

Experiments were performed to determine the effect of the total current, acid type, electrolyte temperature, particle size and % FeS_2 contamination on the reduction of chalcopyrite.

4 M HCl, 4 M $HClO_4$, 2 M H_2SO_4 and 2.7 M H_3PO_4 were all investigated as possible catholytes for the reduction of chalcopyrite. Table 3 shows the measured cell voltages using various electrolytes. H_3PO_4 was excluded after one experiment due to its low conductivity. The other acids exhibited satisfactory cell voltages and were used in later experiments.

During reduction experiments it was found that the initial current efficiency, based on the stoichiometry of reaction (1), was generally less than 60 %. The remaining current was consumed by H_2 evolution,

$$H^+ + e^- \longrightarrow 1/2\ H_2 \qquad (54)$$

Table 3. Total cell voltage during reduction and oxidation experiments

Experiment #	Type Experiment	Total Cell Voltage, V	Electrolyte Composition	Total Cell Current,A
E-116 (3)	Reduction	4.5-5.0	4 M HCl	10
E-116B (3)	Oxidation	4.0-4.6	4 M HCl	10
E-112 (3)	Reduction	5.5-6.5	4 M HCl	19.5
E-112B (3)	Oxidation	5.5-5.9	4 M HCl	19.5
E-92 (3)	Reduction	5.5-7.0	4 M HCl	28.5
E-92B (3)	Oxidation	5.7-6.3	4 M HCl	28.5
E-132 (3)	Reduction	6.6-7.7	4 M HCl	30
E-132B (3)	Oxidation	6.7-6.9	4 M HCl	30
E-98 (3)	Reduction	8.1-8.7	4 M HCl	40
E-98B (3)	Oxidation	7.4-8.6	4 M HCl	40
E-104 (3)	Reduction	8.6-9.3	4 M HCl	53
E-104B (3)	Oxidation	8.5-10.0	4 M HCl	53
E-154 (3)	Reduction	7.8-8.6	4 M H_2SO_4	40
E-154B (3)	Oxidation	9.0-10.5	4 M H_2SO_4	40
E-164 (3)	Reduction	7.8-8.6	4 M $HClO_4$	40
E-164B (3)	Oxidation	9.0-10.5	4 M $HClO_4$	40
E-174 (3)	Reduction	7.8-8.6	2.7 M H_3PO_4	10
E-174B (3)	Oxidation	9.0-10.5	2.7 M H_3PO_4	10

and by a small amount of elemental copper formation,

$$Cu_{1.8}S + 2\ H^+ + 2\ e^- \longrightarrow 1.8\ Cu + H_2S \qquad (55)$$

Most reduction experiments were stopped when approximately 30-35% of the $CuFeS_2$ had reacted. This led to Fe (II) concentrations on the order of 0.1 M and dissolved copper concentrations of less than 0.0001 M. As shown in Figure 6, the dissolved copper concentration decreased rapidly with time, leveling off at about 10^{-5} M. This decline was expected, since dissolved copper is not stable in the presence of a cathodic electrode.

Two methods were used to determine the current supporting reaction (55): The first method consisted of measuring the total moles of Fe dissolved, calculating the expected weight of the final solid product (based on reaction (1) only) and subtracting the actual weight of the final product. This gave the value for the amount of sulfur reduced according to reaction (55), and hence the current for reaction (55). However, within the limits of experimental error, it could not be determined if reaction (55) even occurred (on some occasions elemental Cu was qualitatively identified by visual inspection of the solid product through the walls of the reactor). The second technique used for determining the extent of occurrence of reaction (55) consisted of measuring the ratio of H_2:H_2S exiting the reactor, using a gas chromatograph. However, the ratio could not be determined accurately enough to give any conclusive results. The major problem preventing the accurate determination of the ratio of gases was the high solubility of

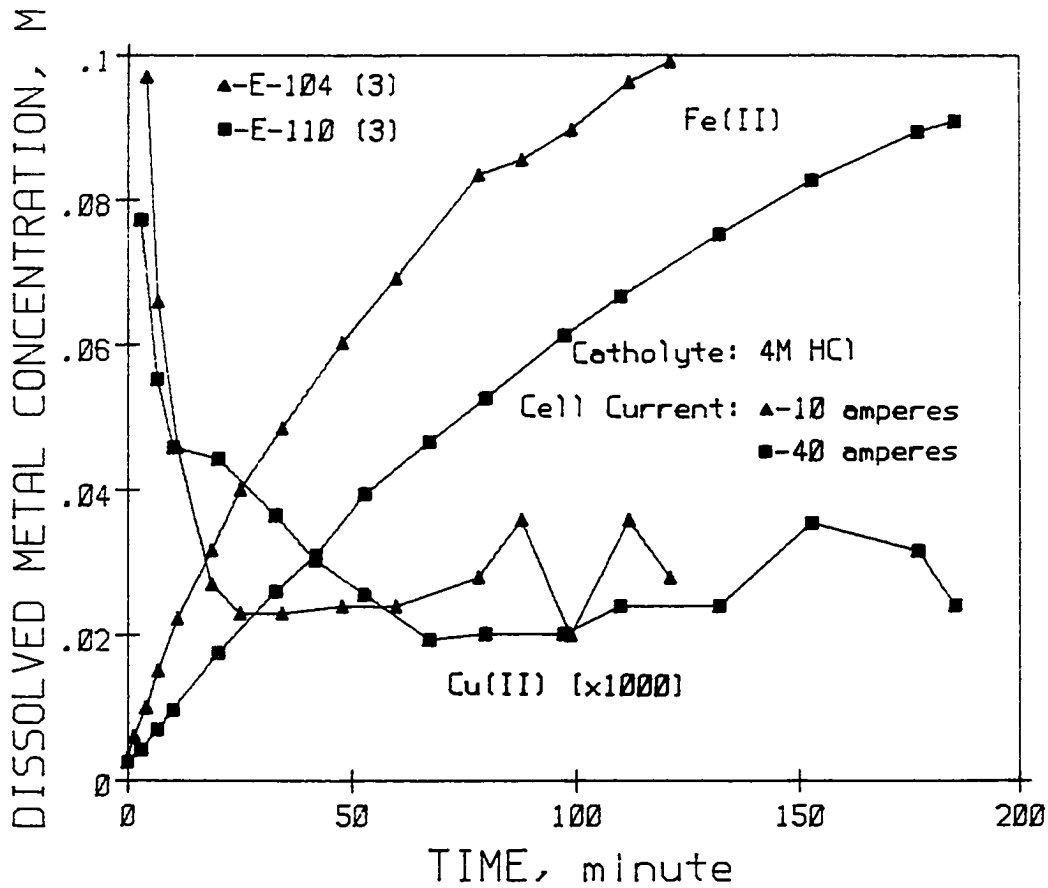

Figure 6. Comparison between the dissolved Fe and Cu concentrations during the reduction of $CuFeS_2$

H_2S in the acid electrolyte. The failed attempts at determining the individual fraction of the current supporting reactions (55) were most likely an indication of the insignificance of the reaction.

FeS_2 is one of the major impurities found in $CuFeS_2$. The main reaction that occurred during the attempted reduction of FeS_2 was the evolution of H_2. Only a small portion of the total current was actually consumed by the cathodic dissolution of FeS_2.

$$FeS_2 + 4\ H^+ + 2\ e^- \longrightarrow Fe^{2+} + 2\ H_2S \qquad (56)$$

The experimental results indicated that over 99 % of the cathodic current was consumed by H_2 evolution during FeS_2 reduction in 4 M HCl, at 40 amps total cell current. This was expected, since the overpotential for the evolution of H_2 on FeS_2 is only 260 mV at 1 mA/cm^2 of H_2 generated [11].

A porous product layer of $Cu_{1.8}S$ encapsulated the shrinking $CuFeS_2$ core as $CuFeS_2$ was cathodically dissolved. The adhesion between the product layer and the unreacted core was an important factor in the first stage of the proposed $CuFeS_2$ dissolution process. Production of a nonadherent product layer would mean that a filtering system would have to be used to collect the $Cu_{1.8}S$ for use in the second stage of the process. The material that did not adhere to the unreacted $CuFeS_2$ was washed out of the reactor and settled in the catholyte reservoir. Chemical analysis of the 'reservoir material' showed that it contained 10-15 times more copper than iron, indicating that it was composed mostly of fragments of the $Cu_{1.8}S$ product layer. The results in Table 4 indicate that the

Table 4. $CuFeS_2$ reduction product layer cohesiveness

Experiment #	Electrolyte Composition	Total Cell Current,A	% Product Layer Remaining on the Unreacted $CuFeS_2$
E-116 (3)	4 M HCl	10	83.3
E-110 (3)	4 M HCl	19.5	75.3
E-92 (3)	4 M HCl	28.5	77.3
E-98 (3)	4 M HCl	40	75.7
E-104 (3)	4 M HCl	53	69.2
E-154 (3)	4 M H_2SO_4	40	66.5
E-164 (3)	4 M $HClO_4$	40	86.6
E-174 (3)	2.7 M H_3PO_4	10	79.5

cohesiveness of the product layer may have been a function of electrolyte composition. Depending on the composition of the electrolyte, about 65-85% of the $Cu_{1.8}S$ that was produced, remained attached to the unreacted $CuFeS_2$. However, more experiments would have to be done to test this hypothesis. As can be seen in Table 4, the cell current had a large effect on the amount of reservoir material produced. Possibly the increased particle bed agitation, caused by the rapid evolution of H_2S and H_2 at high cell currents, was responsible for the increase in reservoir material with increasing current. The reason for the difference in product layer adhesion is not readily apparent.

The photographs of cross sectioned samples of reduced chalcopyrite particles shown in Figure 7 indicate that the $Cu_{1.8}S$ product layer's structure depended on the electrolyte composition. The photographs show that the $Cu_{1.8}S$ product layer is made up of individual particles that are on the order of 1 micron for 4 M HCl and less than 0.1 micron for the other electrolyte acids used. It also appears that the product layer produced in 4 M HCl has larger pores than the other product layers.

The scanning electron micrographs in Figure 7 indicate that the product layer produced, when using a 4 M HCl electrolyte, is composed of more crystalline particles than the product layers produced using the other electrolytes. The different product layer structures may have been the reason for the variation in the product layer adherency in relation to the electrolyte acid used (Table 4).

Most reports in the literature state that the reduction of $CuFeS_2$ yields Cu_2S. The product composition was usually determined by measuring

Figure 7. Scanning electron micrographs and cross sectional photographs of the product layer formed during the reduction of $CuFeS_2$ in 2 M H_2SO_4 (E-67 (2)), 4 M HCl (E-73 (2)) and 4 M $HClO_4$ (E-87 (3))

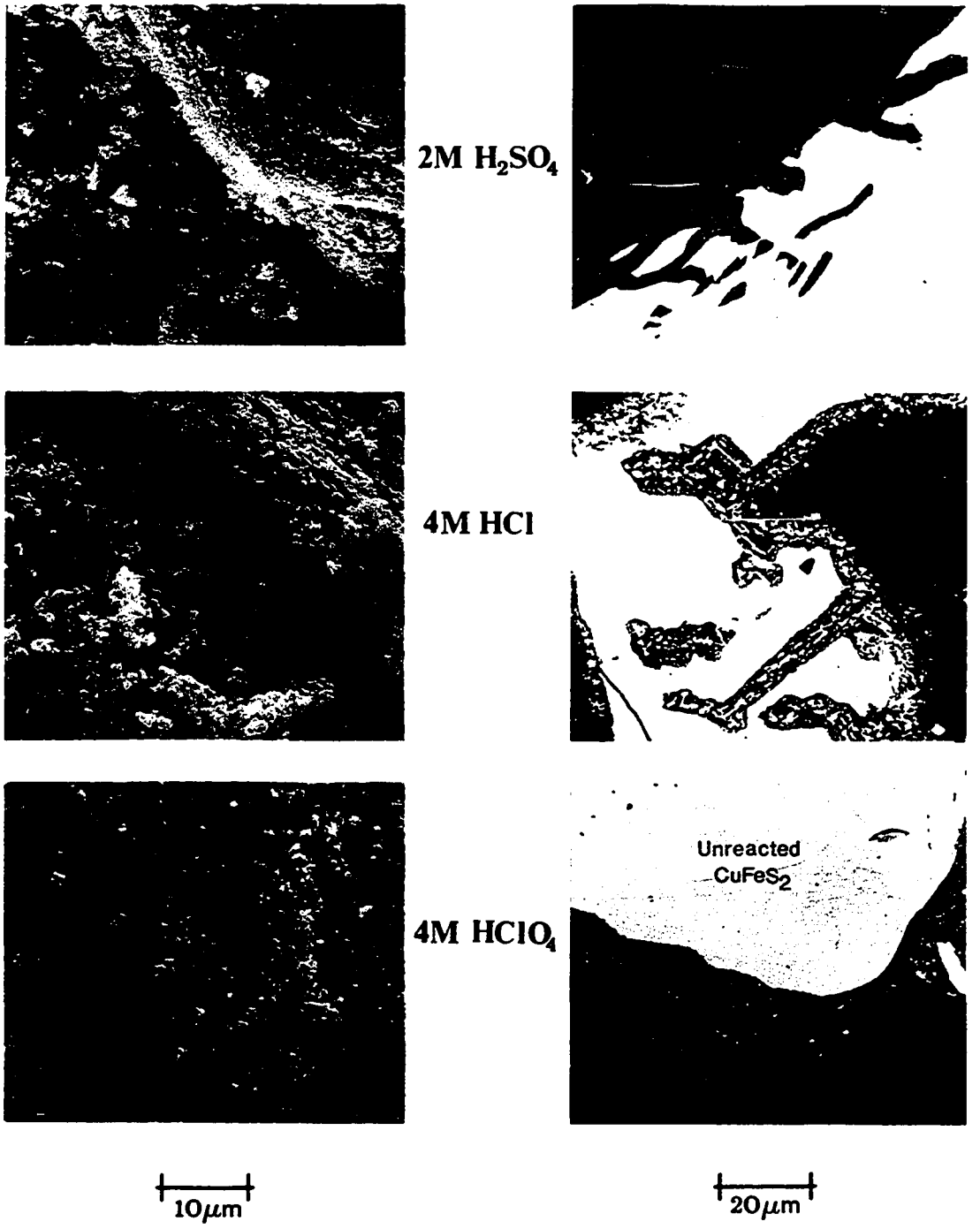
2M H_2SO_4
4M HCl
4M $HClO_4$
Unreacted
$CuFeS_2$
10μm
20μm

the weight percent copper or by comparing x-ray powder diffraction spectra. Neither procedure yields very accurate results. In this study, auger electron spectroscopy (AES) was used to determine the composition of the $CuFeS_2$ reduction product layer. AES is a surface sensitive spectroscopy that provides information on only the atoms in the top 10-30 angstroms of the sample. Unfortunately, the auger spectrometer that was employed could only be used to study particles that had a diameter of 1 micron or larger. This meant that only the product layer that was produced in 4 M HCl could be analyzed. The composition of the product layer was determined by comparing its auger spectra to that of pure $CuFeS_2$. The AES results presented in Table 5 show that no Fe was detected in any of the product layer particles that were examined. The detection limit of the instrument for Fe was about 1 atom %. The AES results indicated that the product layer was more likely $Cu_{1.8}S$ than Cu_2S.

Energy dispersion X-ray spectroscopy (EDXS) was performed simultaneously with AES. The EDXS results, also shown in Table 5, indicate that the product layer particles contained about 2-7 atom % Fe. These results, which conflict with the AES results, are misleading because EDXS is not nearly as surface sensitive as AES. The electrons detected using EDXS are indicative of the atomic composition of a volume of the sample which is approximately the size and shape of a 1-10 micron diameter sphere. Any unreacted $CuFeS_2$ that was within the sample volume would have been detected. This would explain why analysis of the particle closest to the unreacted $CuFeS_2$ had the highest measured Fe content. The EDXS analysis gave a copper to sulfur ratio that was slightly less than

Table 5. AES and EDXS elemental analysis results for the $CuFeS_2$ reduction product layer

Sample (Technique)	Distance from $CuFeS_2$ Boundary (micron)	Element	Determined[a] Atom %	Calculated Cu_xS Formula
$CuFeS_2$ (AES)	0	Cu Fe S	25 25 50	-----
Reduction Product (AES)	1.6	Cu Fe S	64.2 ± 0.3 0.0 ± 0.4 35.8 ± 0.2	$Cu_{1.79}S$
Reduction Product (AES)	6.3	Cu Fe S	65.9 ± 0.3 0.0 ± 0.4 34.1 ± 0.2	$Cu_{1.93}S$
Reduction Product (AES)	7.2	Cu Fe S	63.4 ± 0.3 0.0 ± 0.5 36.6 ± 0.2	$Cu_{1.73}S$
$CuFeS_2$ (EDXS)	0	Cu Fe S	27.6 26.0 46.4	$Cu_{1.06}FeS_{1.79}$
Reduction Product (EDXS)	1.6	Cu Fe S	58.7 7.2 34.1	$Cu_{1.72}S$
Reduction Product (EDXS)	6.3	Cu Fe S	62.7 2.2 35.1	$Cu_{1.79}S$
Reduction Product (EDXS)	7.2	Cu Fe S	58.8 2.0 39.2	$Cu_{1.5}S$

[a]The error in the determined atom % using EDXS was approximately 1 % according to the TN-600 manual. The AES determined atom % for each element was calculated by assuming that the N(E)*E values for the unreacted $CuFeS_2$ corresponded to exactly Cu:Fe:S = 1:1:2.

the 1.8:1 expected for digenite. The lower ratio would be expected, though, if the sample volume contained $CuFeS_2$. Although not completely reliable, the EDXS results are in agreement with the more reliable AES results, indicating that the solid product layer was most likely $Cu_{1.8}S$.

X-ray powder diffraction spectra of the chalcopyrite reduction product layers indicated that the composition of the products formed using H_2SO_4 and $HClO_4$ were similar to that formed in HCl. For the purpose of calculating the experimental results, it was assumed that the chemical composition of the chalcopyrite reduction product was not dependent on the catholyte acid used. $Cu_{1.8}S$ was assumed to form in all electrolytes. (The product layer produced using H_2SO_4, $HClO_4$ and H_3PO_4 could very well have been Cu_2S as other researchers have reported.)

Based on the AES and EDXS results, the electrochemical reduction of $CuFeS_2$ is described by the following reaction.

$$1.8\ CuFeS_2 + 5.2\ H^+ + 1.6\ e^- \longrightarrow Cu_{1.8}S + 2.6\ H_2S + 1.8\ Fe^{2+} \qquad (1)$$

B. Chalcopyrite Reduction Experimental Results

It has been argued that the electrolyte composition controls the rate of $CuFeS_2$ reduction, because it determines the solubility of the Fe(II) that is formed [8]. Supposedly when the rate of Fe(II) production exceeds the rate at which Fe (II) can dissolve in the electrolyte and diffuse out of the product layer, the Fe (II) precipitates in the pores of the product layer. The coverage of the unreacted $CuFeS_2$ surface with the

precipitated, nonconductive Fe salt causes the rate of $CuFeS_2$ dissolution to fall and the rate of H_2 evolution to increase. The precipitation argument was tested by cathodically reacting $CuFeS_2$ until the solution contained approximately 0.1 M Fe^{2+}. The electrolyte was then replaced with one containing the exact same H^+ concentration and 0 M Fe^{2+}. The Fe dissolution data from the experiment are shown in Figure 8. No increase in the rate of dissolution was observed when the Fe^{2+} concentration was lowered, indicating that the rate of $CuFeS_2$ dissolution was most likely not limited by diffusion of Fe^{2+} through the product layer.

The solubility argument was also tested by varying the solution temperature. Figure 9 shows that increasing the electrolyte temperature had no effect on the rate of $CuFeS_2$ reduction. Since the solubility of Fe (II) generally increases with temperature, using the precipitation argument explained above, one would expect the rate of chalcopyrite reduction to increase with increasing temperature. Close examination of Figure 9 indicates that there may have even been a slight decrease in the rate of reaction with increasing temperature.

The lack of any temperature influence on the rate of chalcopyrite reduction could be an indication that the activation energies for the competing reactions, $CuFeS_2$ dissolution and H_2, were very similar. If the competing reactions had the same activation energies, then a change in the electrolyte temperature would have effected the reactions equally and no net increase in the rate of H_2 evolution or $CuFeS_2$ dissolution would have been seen.

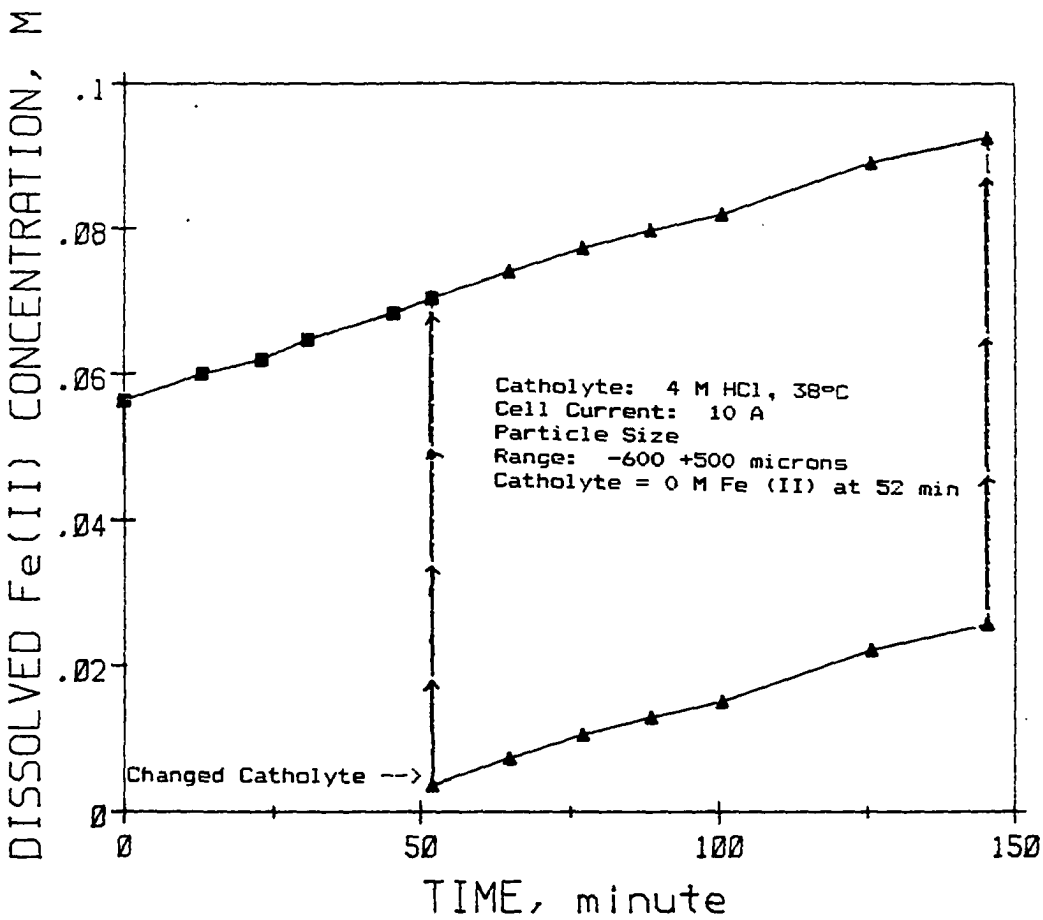

Figure 8. Dependence of the rate of $CuFeS_2$ reduction on the dissolved Fe (II) concentration

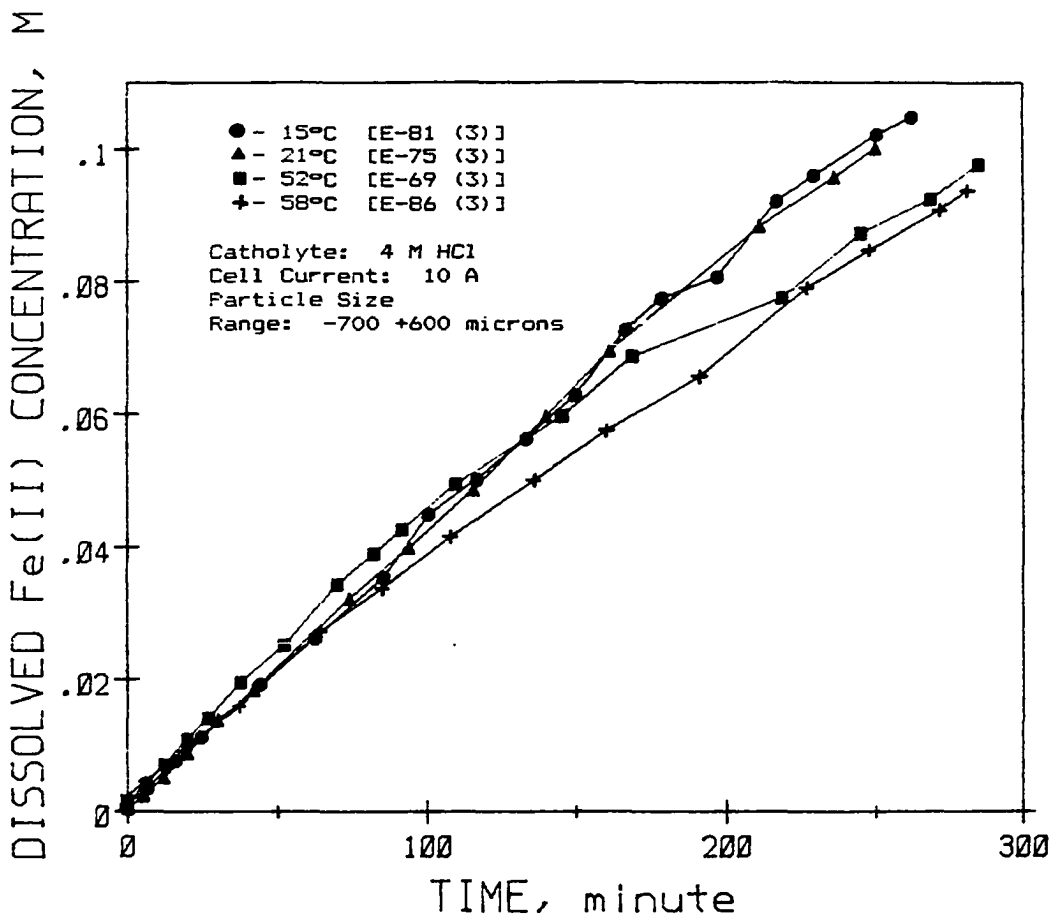

Figure 9. Dependence of the rate of $CuFeS_2$ reduction on temperature

Any model used to explain the reduction of $CuFeS_2$ should agree with the experimental findings that the temperature had no effect on the rate of dissolution and that the rate of $CuFeS_2$ reduction was dependent on the electrolyte composition.

The dissolved Fe concentration versus time data for the experiments designed to determine the effect that the acid anion had on the rate of chalcopyrite dissolution are shown in Figure 10. The catholytes composed of 4 M HCl and 4 M $HClO_4$ resulted in the highest $CuFeS_2$ dissolution rates. The rate of dissolution was considerably less using 2M H_2SO_4. Assuming that the rate of $CuFeS_2$ dissolution depended on the activity of H^+ at the $CuFeS_2$ / electrolyte interface, the dissolution rate results shown in Figure 10 are then in qualitative agreement with the expected H^+ activities, based on the dissociation of the acids. (The order of H^+ dissociation which is $HCl = HClO_4 \gg H_2SO_4 > H_3PO_4$.)

C. Application of Model to the Experimental Results

Values for all the constants in equation (47) are needed before the model equations can be applied to the experimental results. All the constants are known, or can be easily estimated, except for the rate constant K. K must be calculated using equation (41) and the experimentally determined initial fractional current for reaction (1). The initial fractional current was determined from Figure 11 by extrapolating the data for the current efficiency versus time to t = 0. According to the assumptions of the model, the initial fractional

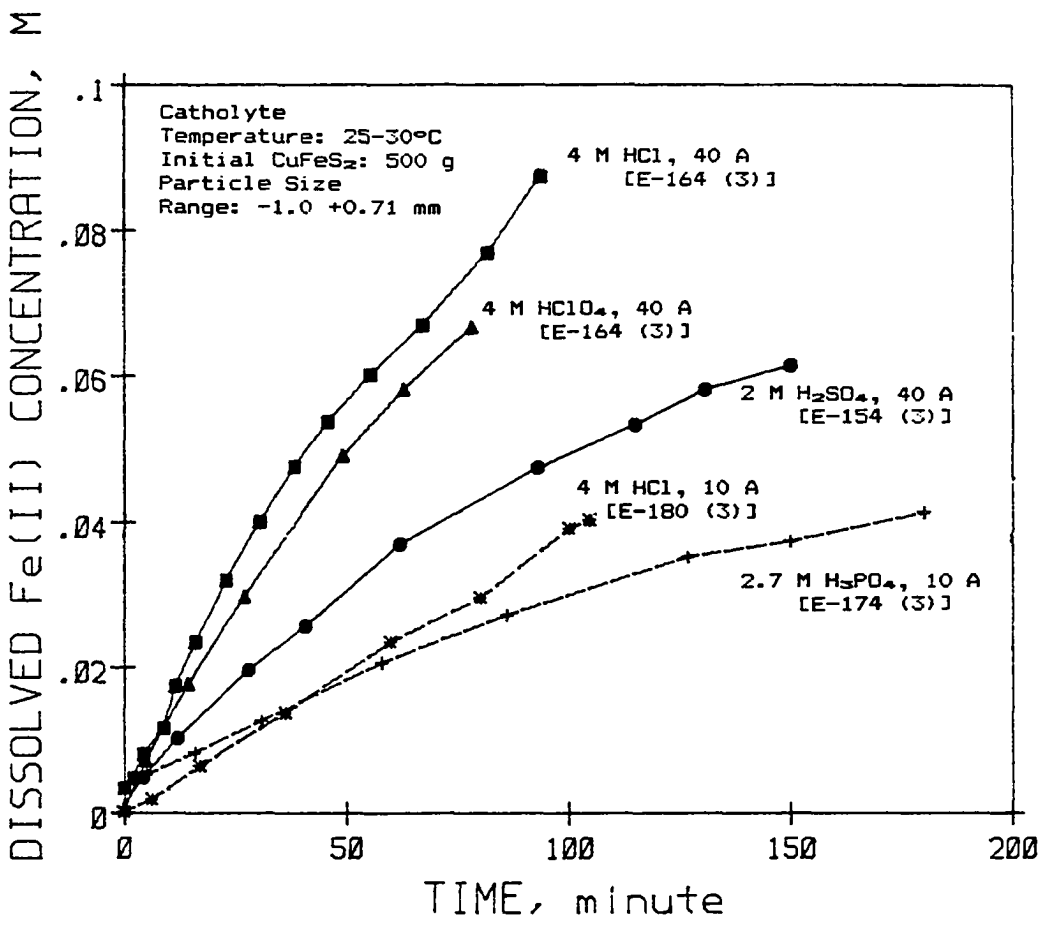

Figure 10. Dependence of the rate of $CuFeS_2$ reduction on the electrolyte composition and total cell current

current should depend only on the bulk concentration of H^+ because no product layer exists at t=0. Figure 11 shows that the fractional current for the reduction of $CuFeS_2$ in 4 M HCl extrapolates to approximately 0.6 at t=0. The decrease in the current efficiency near t=0 was ignored because it was caused by the reduction of the small amount of oxygen that was initially present in the electrolyte. Solving equation (41), using $I_1/I_{total} = 0.6$ and an analytical bulk H^+ concentration of 4 M, gives K = 93750 $cm^6 moles^{-2}$ H^+.

The values that were used for some of the other constants in equation (47) were as follows:

R_o = the average of the + and - screen sizes for the particle size range used.

F = 96484 coulombs / equivalent

$V_{CuFeS2} = 44.1\ cm^3\ mole^{-1}$

N^o_{CuFeS2} = initial moles of $CuFeS_2$ = 2.725 moles for most experiments

C^{bulk}_{H+} = bulk analytical concentration of H^+ = 4 M for all experiments except for 2.7 M H_3PO_4 experiment = 8 M

The diffusion coefficient for H^+ would be expected to be on the order of 10^{-5} cm^2 s^{-1}. The diffusion coefficient value used in the model was smaller than 10^{-5} because it had to account for the porosity and tortuosity of the product layer. A value of 2.6 X 10^{-7} cm2 s^{-1} was chosen by fitting the model to the data for the reduction of chalcopyrite at 28.5 amps.

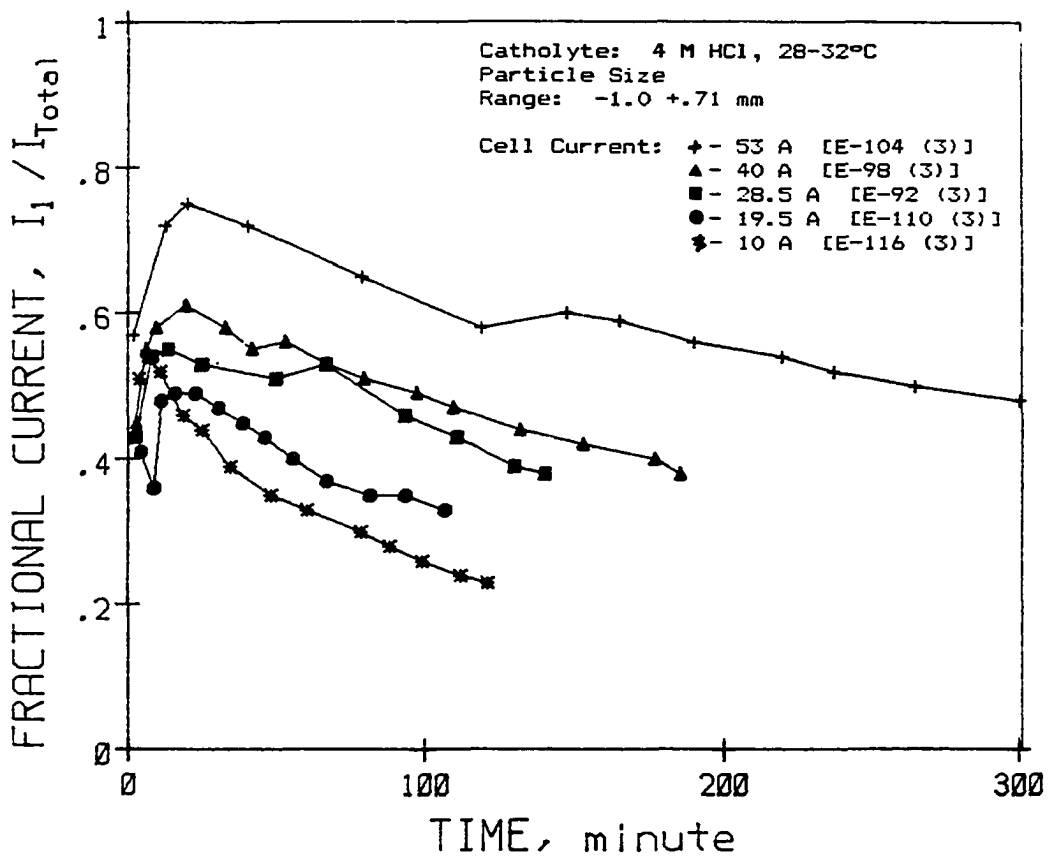

Figure 11. Fractional current versus time data used for the calculation of K_{p-s}

Figure 12 is a plot of the fraction of $CuFeS_2$ reacted versus time for five different cell currents. Considering the complexity of the reduction process, the model agrees quite well with the experimental data.

The model was used to predict the time required for $CuFeS_2$ conversion. These data are shown in Figure 13. The model predicts that above a cell current of approximately 30 amperes, less than 50% of the chalcopyrite will be converted to digenite. Increasing the cell current from 30 to 100 amperes does not increase the initial rate of conversion by very much. But it does cut the final fractional conversion of $CuFeS_2$ by more than 50%.

The predicted H^+ concentration profiles, depicted in Figure 14, indicate why the complete reduction of $CuFeS_2$ is impossible for the conditions listed in the Figure 14. For all cases shown in Figure 14, the model predicts that the H^+ concentration at the surface of the $CuFeS_2$ particle goes to zero before the complete conversion of $CuFeS_2$. At the point where the H^+ concentration goes to zero, all of the H^+ is consumed by H_2 evolution. The boundary layer can move no farther into the particle because the rate of H^+ diffusion equals the rate of consumption due to H_2 evolution.

Figure 15 is a plot of the model equation and the experimental data for the fraction of $CuFeS_2$ reacted versus time for the reduction of chalcopyrite in different electrolytes. The rate constants for the reduction of $CuFeS_2$ in each of the different electrolytes were determined by extrapolating the fractional current versus time data to t=0, for each electrolyte system. The same D_{H+} value was used for all the model

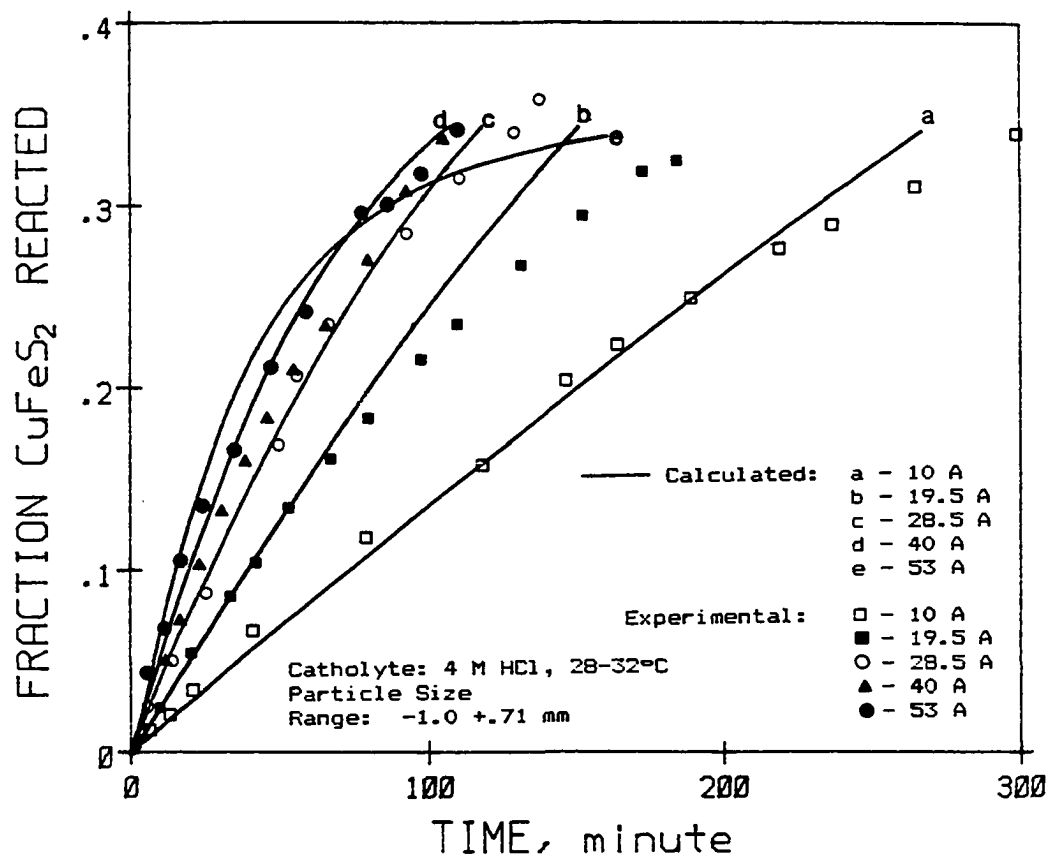

Figure 12. Comparison between the experimental and predicted fraction of $CuFeS_2$ reacted as a function of the total cell current

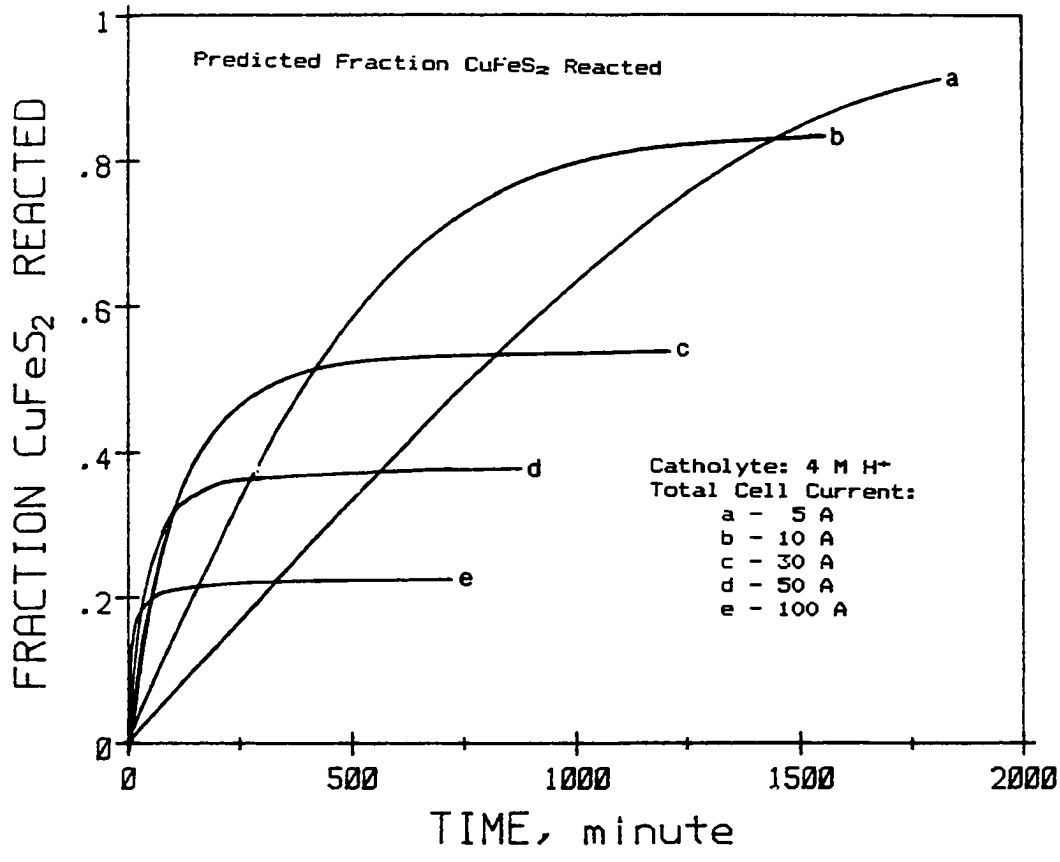

Figure 13. Predicted fraction of $CuFeS_2$ reacted as a function of time and total cell current

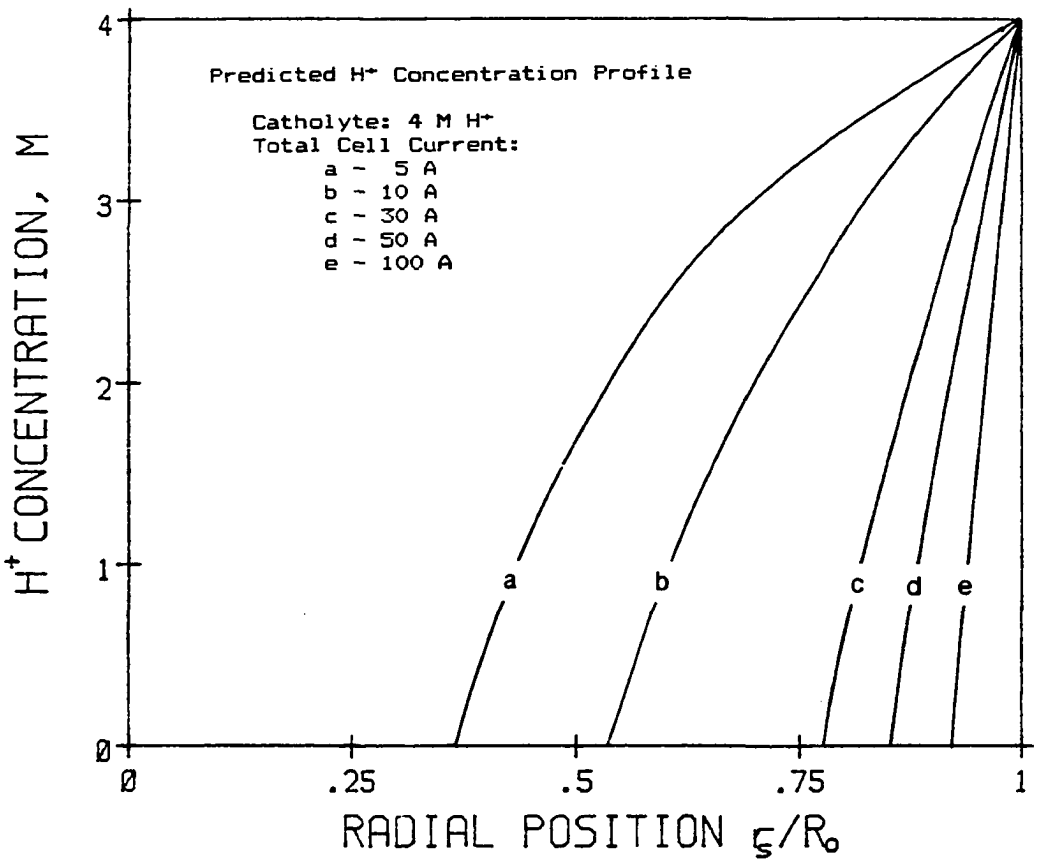

Figure 14. Predicted H^+ concentration profile during the reduction of $CuFeS_2$ at various total cell currents

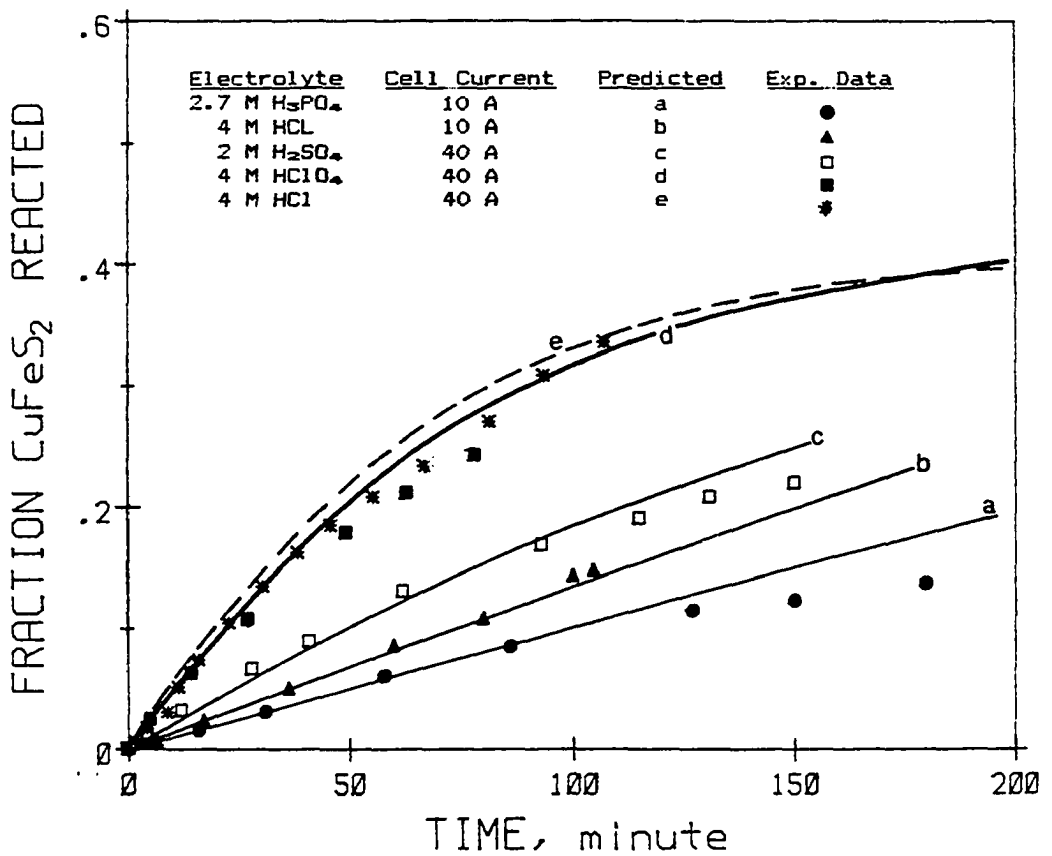

Figure 15. Comparison between the experimental and predicted fraction of $CuFeS_2$ reacted versus time as a function of the electrolyte composition and total cell current

prediction lines in Figure 15, even though the cross sectional photos in Figure 7 indicated that the porosity of the product layer was dependent on the electrolyte composition. Again, the model generally agrees with the experimental data. This agreement supports the hypothesis that the rate of $CuFeS_2$ is controlled by the diffusion of H^+ through the product layer.

The model was also used to predict the time required for the partial conversion of $CuFeS_2$ to $Cu_{1.8}S$; Figure 16. For the case of the different acids, the faster initial conversion rates, are accompanied by smaller final conversion of $CuFeS_2$. This phenomenon is the result of the diffusion limited mass transfer of H^+ to the $CuFeS_2$ surface and the competition for the H^+ by the simultaneously occurring reactions.

The model calculated H^+ concentration profiles, shown in Figure 17, predict that a greater fractional conversion would be obtained by using a higher H^+ concentration and a lower total cell current.

The model's agreement, with the data from the experiments using various cell currents and electrolyte compositions, indicates that the rate of reduction of chalcopyrite is a function of the H^+ concentration at the reaction surface/electrolyte interface and is controlled by the diffusion of H^+ to that interface. The model agreement also indicates that the assumed stoichiometries for the reduction of $CuFeS_2$ and H_2 evolution were correct (reactions (1) and (54), respectively).

The calculated results shown in Figures 14 and 17 imply that the only way an appreciable fraction of the $CuFeS_2$ could be reduced would be by (i) beginning with very small $CuFeS_2$ particles, (ii) continuously or periodically removing the product layer from the unreacted $CuFeS_2$ core or

(iii) using an excessively low cell current so that the H^+ concentration inside the product layer would be close to that of the H^+ concentration in the bulk solution.

D. Operating Parameter Effects on the Reduction of Chalcopyrite

Three experiments were done to determine the effect of the initial radius of chalcopyrite particles on the rate of reduction. The data and calculated model values for the fraction of $CuFeS_2$ reacted versus time, as a function of the initial particle radius, are shown in Figure 18. In this case, the experimental results do not agree very well with the model predicted results, for the smallest particles used. The discrepancy could have been caused by the lowering of the catholyte flow rate, which was necessary when using the smallest particles in order to prevent the particles from being swept out of the reactor. Because of the lower electrolyte flow rate, the hydrodynamic boundary layer probably added significantly to the resistance of the diffusion of H^+ to the reacting surface. The model did not account for the additional resistance.

The reduction of $CuFeS_2/FeS_2$ mixtures was investigated to determine the effect that FeS_2 contamination of the $CuFeS_2$ would have on the efficiency of the proposed process. The Fe dissolution rate results for the reduction of $CuFeS_2/FeS_2$ mixtures are shown in Figure 19. Figure 19

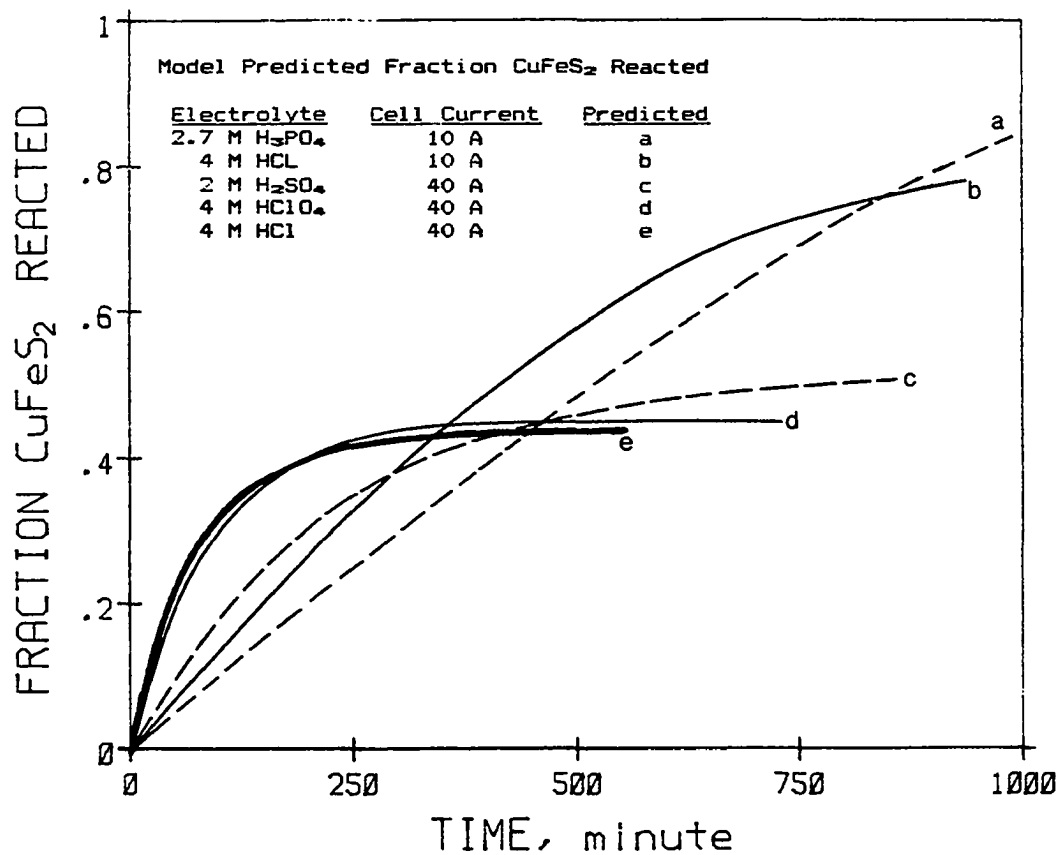

Figure 16. Predicted fraction of $CuFeS_2$ reacted as a function of time, electrolyte composition and total cell current

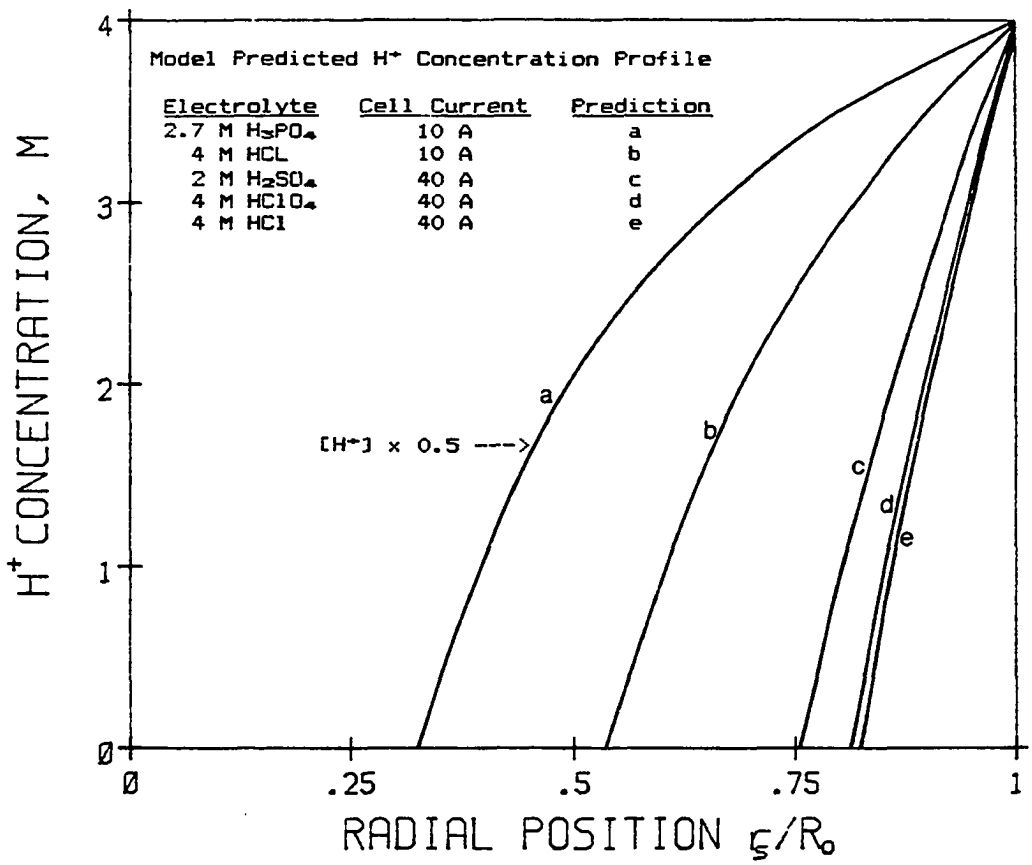

Figure 17. Predicted H^+ concentration profile during the reduction of $CuFeS_2$ for electrolyte compositions and total cell currents

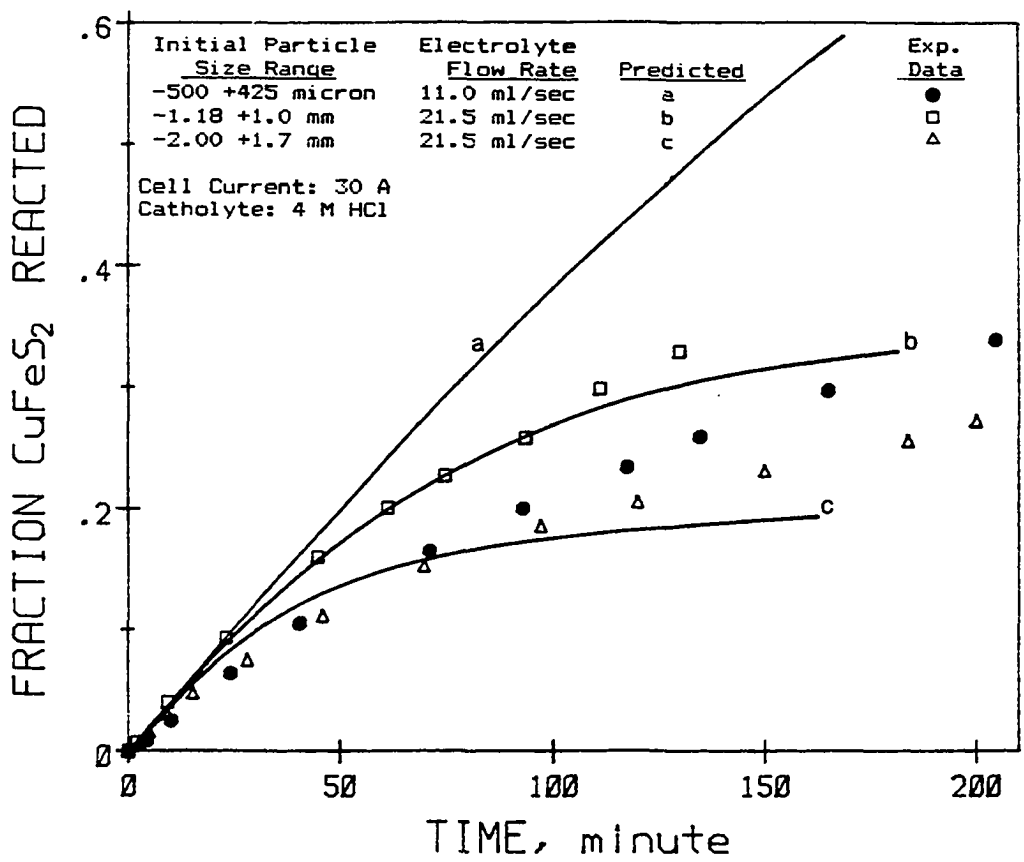

Figure 18. Comparison between the experimental and predicted fraction of $CuFeS_2$ reacted as a function of the initial particle size range

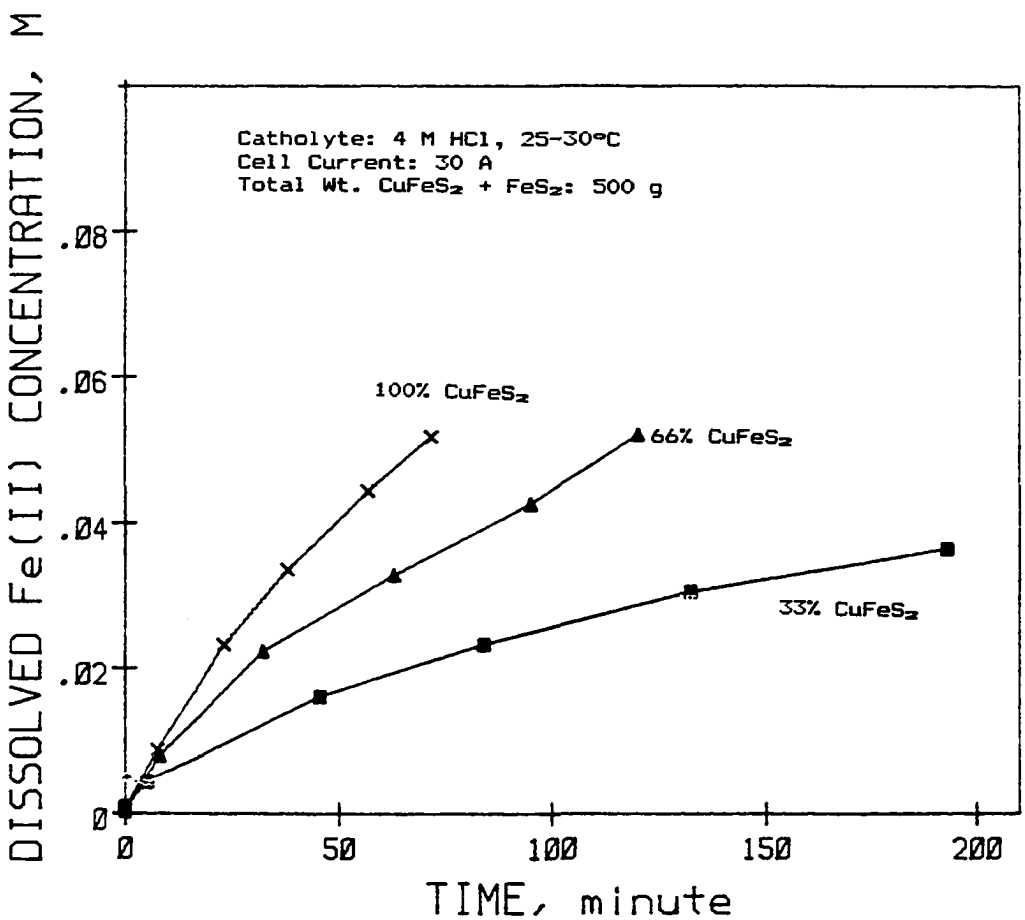

Figure 19. Dependence of the rate of $CuFeS_2$ reduction on the percent of FeS_2 contamination

indicates that FeS_2 has a detrimental effect on the rate of $CuFeS_2$ reduction, as measured by the rate of Fe dissolution. This is because FeS_2 is a good material for generating H_2. When the data in Figure 19 are expressed in terms of the fraction of $CuFeS_2$ reacted, Figure 20, then there appears to be very little effect due to the presence of FeS_2. Apparently, FeS_2 consumes a portion of the current that is approximately equal to its weight fraction of the total particulate bed. The implication of Figure 20 is that the reduction of an individual chalcopyrite particle is not disturbed by the presence of FeS_2.

E. Electrochemistry Related to the Oxidation of the Chalcopyrite Reduction Product Layer

The anodic dissolution of the $Cu_{1.8}S$ product layer, which resulted from the reduction of $CuFeS_2$, was complicated by the presence of the underlying $CuFeS_2$ core. The oxidation electrochemistry turned out to be strongly dependent on the electrolyte composition and the total cell current. Under some experimental conditions, Cu (I) was a major dissolution product.

Preliminary oxidation experiments were performed using natural specimens of Cu_2S. The Cu_2S was oxidized in an anolyte of 4 M HCl. The Cu species concentrations versus time data in Figure 21, indicate that Cu (I) was the major product of Cu_2S oxidation. The line representing the Cu (I) concentration was calculated from the difference in the total Cu concentration and the Cu (II) concentration. In Figure 21, the Cu (II) and Cu (I) concentrations are only shown for part of the experiment. This

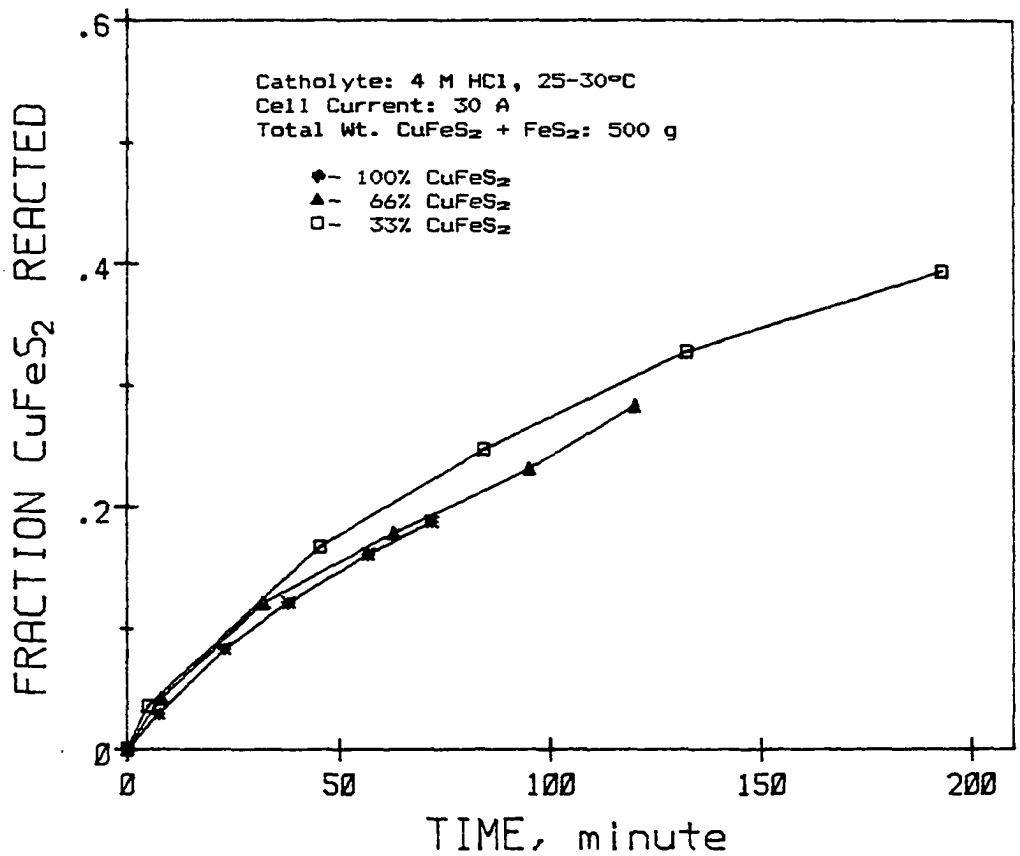

Figure 20. Dependence of the fraction of $CuFeS_2$ reacted on the percent of FeS_2 contamination

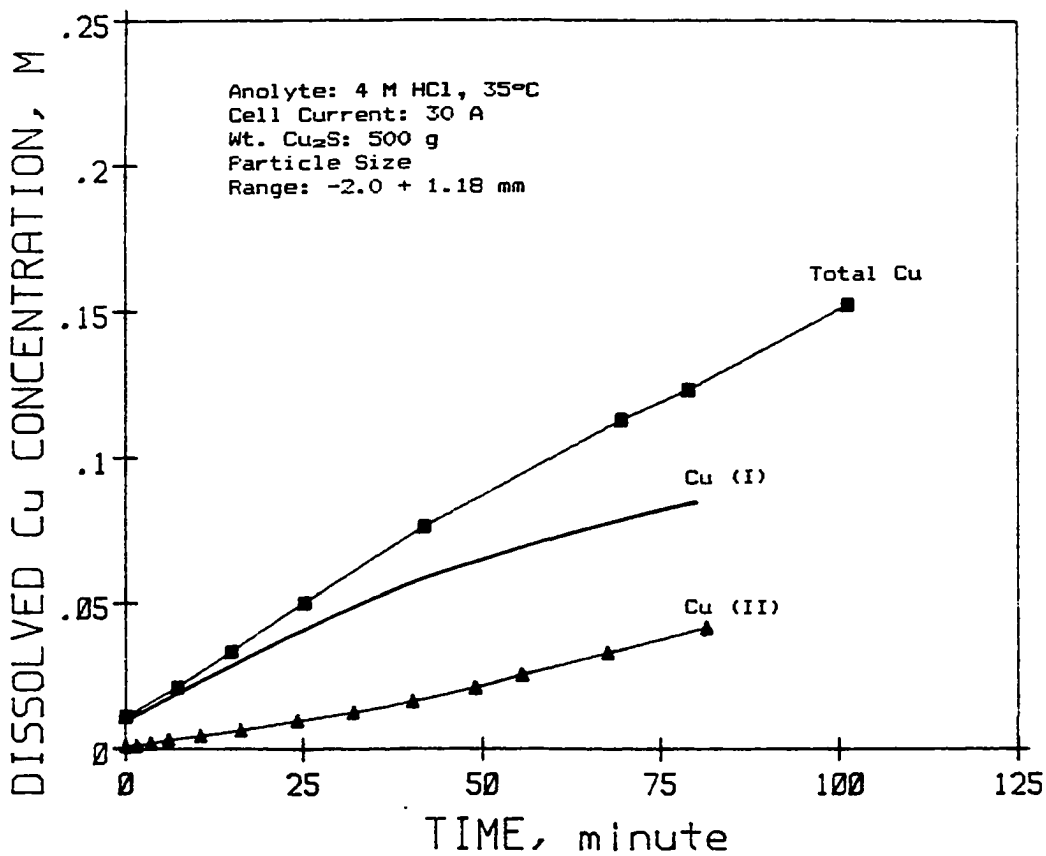

Figure 21. Cu species concentrations during the oxidation of natural chalcocite in 4 M HCl

is because the spectrometer that was used to measure the Cu (II) concentration could only measure up to approximately 0.8 M Cu (II).

To date, there have been no reports in the literature on the formation of Cu (I) during the anodic dissolution of Cu_2S. Dissolving Cu_2S as Cu (I) requires only half of the electrons that are needed when Cu (II) is the dissolving species. (The subsequent deposition of copper from Cu (I) would also require only half of the number of electrons.) The successful production of Cu (I) was due to the fact that Cu (I) forms stable chloride complexes [35].

The anodic dissolution of the $Cu_{1.8}S$ product layer in 4M HCl was also found to produce Cu (I) by the following reaction.

$$Cu_{1.8}S \longrightarrow CuS + 0.8\ Cu^{+} + 0.8\ e^{-} \qquad (2)$$

The total Cu and Cu (II) species concentrations versus fraction time, for two $Cu_{1.8}S$ product layer oxidation experiments, are shown in Figure 22. The Cu (I) concentration is just the difference between the total Cu concentration and the Cu (II) concentration. No Cl_2 evolution was detected while Cu (I) was being generated. When the metal phase composition approached CuS, Cu (I) production ceased, Cl_2 evolution began, elemental sulfur was formed and the Cu (I) in solution was rapidly oxidized to Cu (II). The production of Cl_2 prevented the formation of stable Cu (I) complexes because dissolved Cl_2 readily oxidizes the Cu (I) to Cu (II).

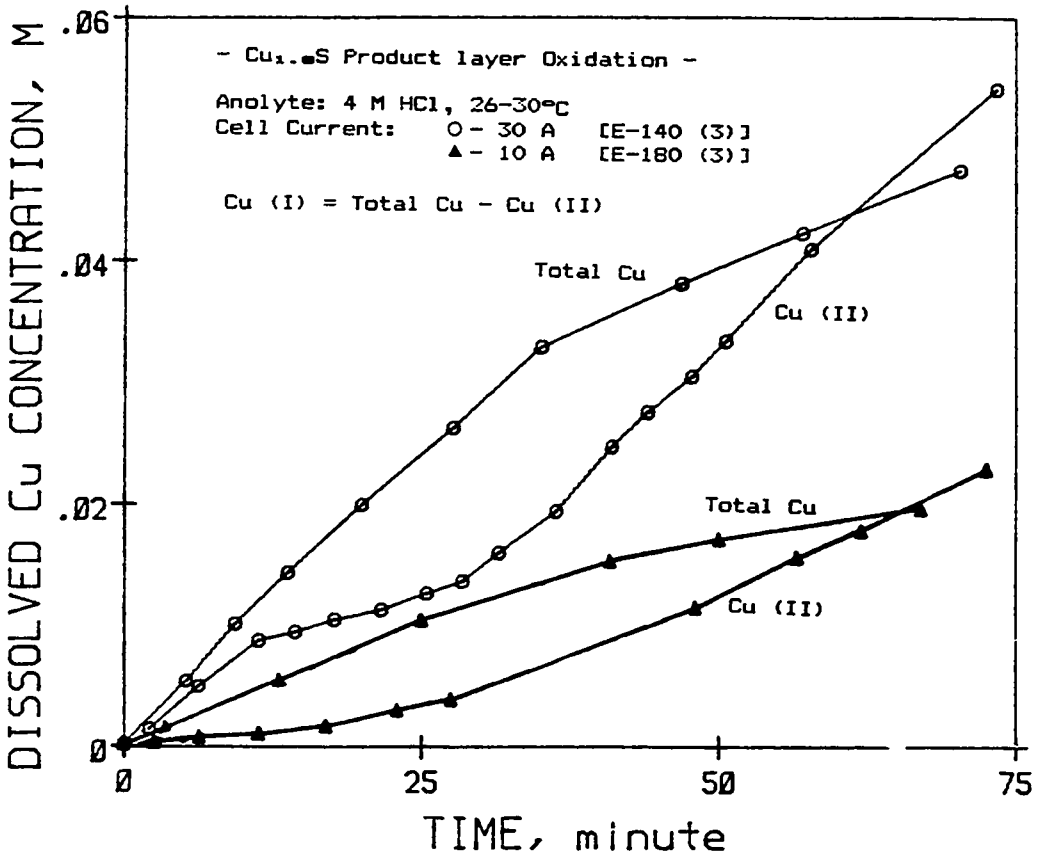

Figure 22. Cu species concentrations during the oxidation of the $CuFeS_2$ reduction product layer in 4 M HCl

Figures 23 and 24 reveal the effect of the electrolyte composition on the initial rate of dissolution of the $Cu_{1.8}S$ product layer. The initial rate of dissolution was fastest in 4 M HCl because of the formation of Cu (I). The reason that the rate of dissolution is so much slower in the other electrolytes is because Cu (II) was the dissolution product. Cu (I) was never detected in the 2M H_2SO_4, 4M $HClO_4$ or 2.7 M H_3PO_4 electrolytes.

In all solutions investigated, except 4 M HCl, $Cu_{1.8}S$ dissolution was accompanied by steadily increasing oxygen evolution. As expected from the reports in the literature [38,39], no elemental sulfur was ever detected unless the electrolyte contained Cl^-.

Figures 23 and 24 show that the rate of copper dissolution decreased as the solid product stoichiometry approached CuS, when an electrolyte composed of 2 M H_2SO_4, 4M $HClO_4$ or 2.7 M H_3PO_4 was used. After most of the original $Cu_{1.8}S$ had reacted to form CuS, O_2 evolution became the major reaction. Addition of Cl^- to the electrolyte caused the evolution of O_2 to be replaced by the production of chlorine gas. During all of the oxidation experiments, the production of elemental sulfur was accompanied by the evolution of Cl_2. A rise in the current efficiency and the production of S^o was evidence that the CuS was oxidized once the Cl^- was added. It was thus concluded that without Cl^-, $Cu_{1.8}S$ would only dissolve as far as CuS.

$$Cu_{1.8}S \longrightarrow CuS + Cu^{2+} + 2e^- \qquad (57)$$

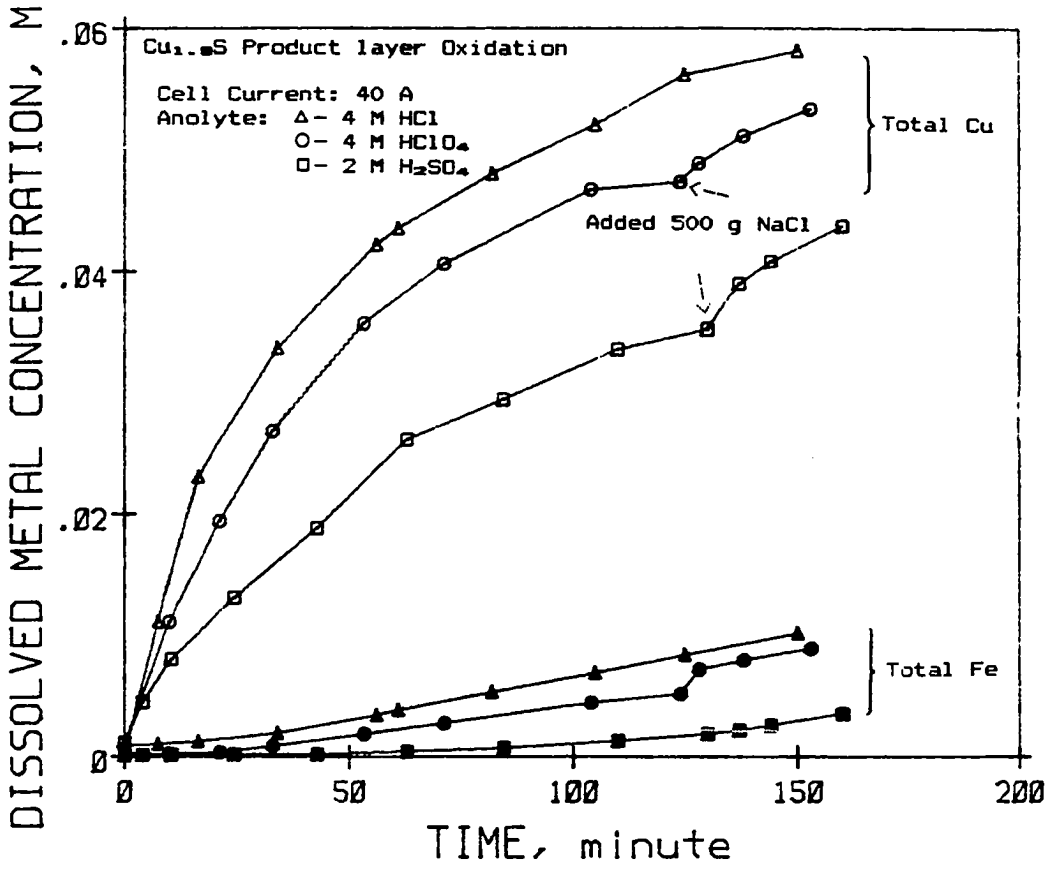

Figure 23. Dependence of the rate change of the total Cu and total Fe concentrations on the electrolyte composition for the oxidation of the $CuFeS_2$ reduction product layer

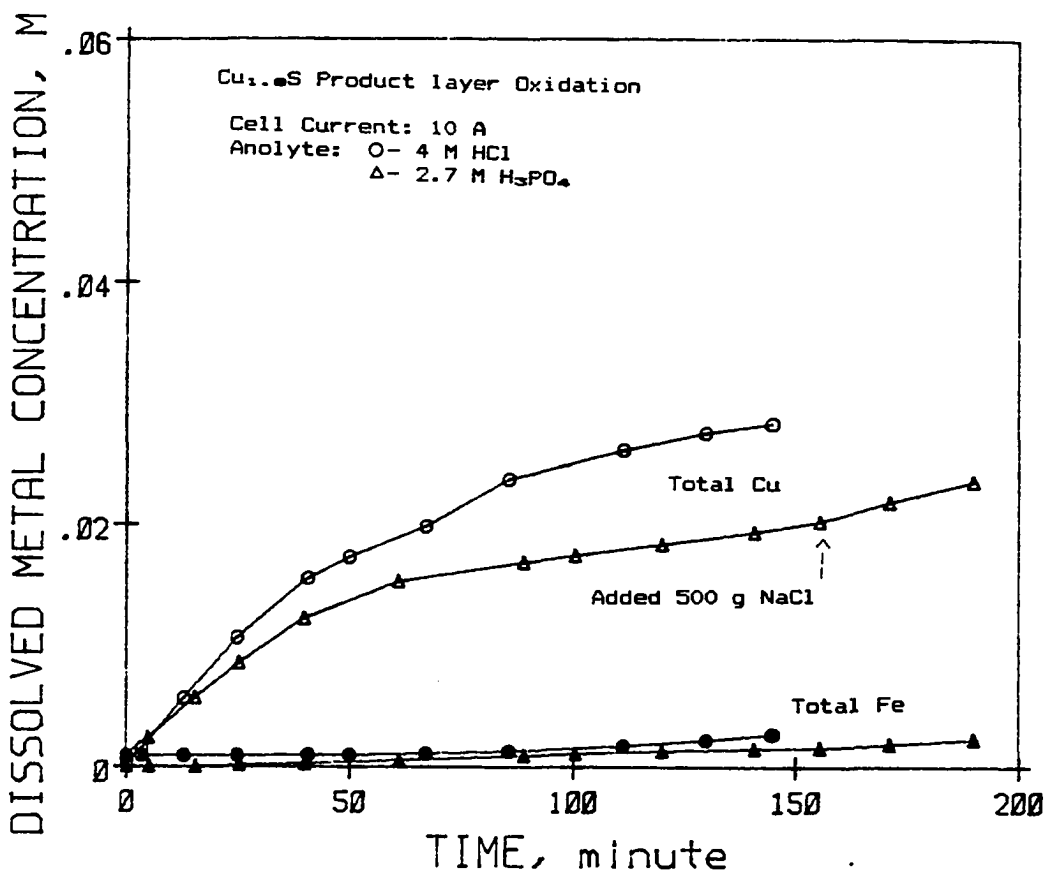

Figure 24. Dependence of total Cu and total Fe concentrations on the electrolyte composition during the oxidation of the $CuFeS_2$ reduction product layer

The increase in rate of copper dissolution that resulted from the addition of Cl^- to the H_2SO_4 , $HClO_4$ and H_3PO_4 electrolytes was most likely due to the formation of copper-chloride complexes and the evolution of Cl_2.

The formation of copper-chloride complexes would have had the effect of lowering the oxidation potential for the dissolution of $Cu_{1.8}S$ and CuS. The lower oxidation potential would then have caused the rate of copper sulfide dissolution to increase relative to the side reactions (provided that the side reactions were not also functions of the Cl^- concentration).

Cl_2 is known to oxidize CuS, Cu_2S and $CuFeS_2$ [17]. The Cl_2 that was electrochemically generated on the surface of the copper sulfide would have reacted with the copper sulfide, increasing the rate of Cu dissolution. Apparently, the oxidation of the copper sulfides with O_2 is much slower than with Cl_2, despite oxygen's higher oxidation potential.

The Fe concentrations are also shown in Figures 23 and 24. The iron dissolution is indicative of the dissolution of $CuFeS_2$. The increase in the Fe dissolution rate that occurred when NaCl was added to the electrolyte corresponded to the advent of Cl_2 evolution. The indiscriminate oxidation of $CuFeS_2$ by Cl_2 would account for the the increase in the rate of Fe^{2+} dissolution after Cl^- was added to the electrolyte. The rise in the electrolyte Fe concentration would also have accounted for the disappearance of the Cu (I) because Fe (III) reacts very quickly with Cu (I) to form Cu (II) and Fe (II).

$$Fe^{3+} + Cu^{+} \longleftrightarrow Fe^{2+} + Cu^{2+} \qquad (58)$$

The Fe (II) that was formed by reaction with Cu (I) could have been oxidized at the electrode surface to form more Fe (III) and reacted with more Cu (I). It is obvious that a small amount of dissolved Fe could prevent any significant amount of Cu (I) from forming.

The only way to eliminate the production of Fe (III), that resulted from $CuFeS_2$ oxidation, would be by 100% reduction of the $CuFeS_2$ in the first stage, or by separating the reduced product layer from the unreacted $CuFeS_2$ core by grinding or some similar method.

Shown in Table 6 are the results of an experiment that was performed to determine the composition of solid that resulted from the separation of the $Cu_{1.8}S$ product layer and the unreacted $CuFeS_2$ core by agitating the particles in an ultrasonic bath. The resulting fractured product layer was separated from the unreacted $CuFeS_2$ by suspending the $Cu_{1.8}S$ in solution and decanting the liquid. The product layer material was then dissolved in aqua regia. The chemical dissolution results shown in Table 6 indicate that the removed product layer material contained about 70-85% $Cu_{1.8}S$. There was a slight variation in the chemical composition of the removed reduction product layer with catholyte composition, but in all cases some Fe was detected. The chemical compound in the product layer that contained the iron was identified as $CuFeS_2$ using x-ray powder diffraction. The unreacted $CuFeS_2$ was the result of the crude separation process used. The contamination of the product layer with Fe is undesirable because it would result in the simultaneous dissolution of Fe with Cu when the removed product layer material was oxidized.

Table 6. Chemical analysis for ultrasonically removed chalcopyrite reduction product layer

Experiment	Electrolyte	Cu:Fe (mole ratio)	Mole % $Cu_{1.8}S$
E-67 (2)	2 M H_2SO_4	5.27	70.3
E-73 (2)	4 M HCl	13.15	87.1
E-87 (2)	4 M $HClO_4$	8.55	80.7
E-174 (3)	2.7 M H_3PO_4	5.68	72.2

A series of scanning electron micrographs of the surface of the reduced chalcopyrite particles are shown in Figures 25 and 26. The micrographs clearly show that no elemental sulfur formed until after the Cl^- was added to the electrolyte. The increase in the porosity of the product layer, with increasing removal of Cu from the solid phase, is very evident. No significant rise in the cell voltage was detected when the sulfur layer formed. It is possible that the elemental sulfur layer was porous enough that electrical contact between the particles was maintained. But it is more likely that the current feeder electrodes provided a large enough surface area for the oxidation of Cl^- to Cl_2, which in turn chemically oxidized the CuS. The conductivity of the particles would not matter in this case.

F. Operating Parameter Effects on the Oxidation of the Chalcopyrite Reduction Product Layer

Based on the initial results for the anodic dissolution of $Cu_{1.8}S$, 4 M HCl was chosen as the anolyte acid. Further anodic dissolution experiments, designed to test the effect that the variation of the cell current, temperature, particle size range and % FeS_2 contamination had on the anodic dissolution of the $Cu_{1.8}S$ product layer, were performed using only 4 M HCl.

A separate experiment was performed to determine if Cu (I) was one of the dissolved products produced during the oxidation of $CuFeS_2$ in 4 M HCl. Figure 27 shows that the measurement of the Fe (III) and Cu (II) concentrations indicated no Cu (I) or Fe (II) was formed. Cl_2 evolution

Figure 25. Scanning electron micrographs of $CuFeS_2$ particles at various stages of reaction

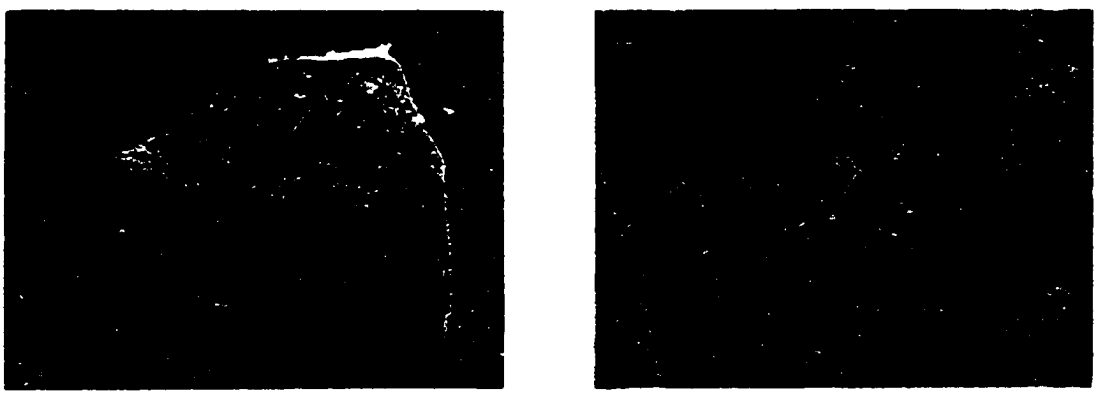

Unreacted $CuFeS_2$

200 μm

$Cu_{1.8}S$ Product Layer
Catholyte: 4M HCl

CuS Product Layer
Anolyte: 2M H_2SO_4

Sulfur Product Layer
Anolyte: 2M H_2SO_4 + 0.75M NaCl

Figure 26. Scanning electron micrographs of $CuFeS_2$ particles at various stages of reaction

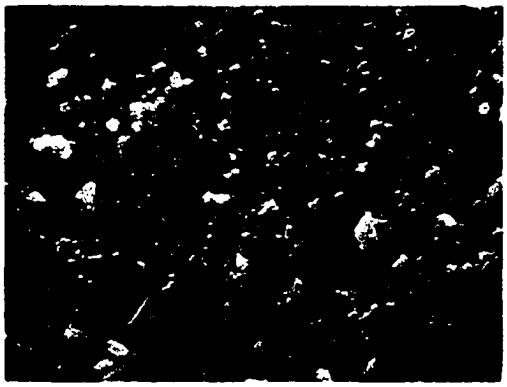

Unreacted $CuFeS_2$

$Cu_{1.8}S$ Product Layer
Catholyte: 4M HCl

10 μm

CuS Product Layer
Anolyte: 2M H_2SO_4

Sulfur Product Layer
Anolyte: 2M H_2SO_4 + 0.75M NaCl

Figure 27 also indicates that there was a slightly greater rate of Fe dissolution compared to that of Cu. This phenomenon was probably the result of FeS_2 contamination of the $CuFeS_2$ and not the result of the selective dissolution of Cu over Fe. Measurement of the total dissolve Fe and Cu concentrations versus time and the observed formation of elemental sulfur during the anodic oxidation of $CuFeS_2$ in 4 M HCl indicated that $CuFeS_2$ dissolved according to the following reaction.

$$CuFeS_2 \longrightarrow Cu^{2+} + Fe^{3+} + S^o + 5\ e^- \qquad (59)$$

Figure 28 shows the porous elemental sulfur layer on a reacted $CuFeS_2$ particle. The sulfur layer appears to totally encapsulate the $CuFeS_2$ particle. Total encapsulation of the individual $CuFeS_2$ particles would prevent electrical contact with the current feeder electrodes. The actual mechanism for the dissolution of $CuFeS_2$, once the sulfur layer forms, may have been chemical oxidation by Cl_2, Cu (II) or Fe (III), all of which could have been generated on the current feeder electrode's surface.

Assuming the stoichiometry of reaction (59) was correct, the average current efficiency for the oxidation of $CuFeS_2$ was calculated from the data in Figure 27 to be approximately 40 % at 1.2 A/m^2 (based on the B.E.T. measured surface area of 0.05 m^2/g $CuFeS_2$ and a total cell current of 30 amps).

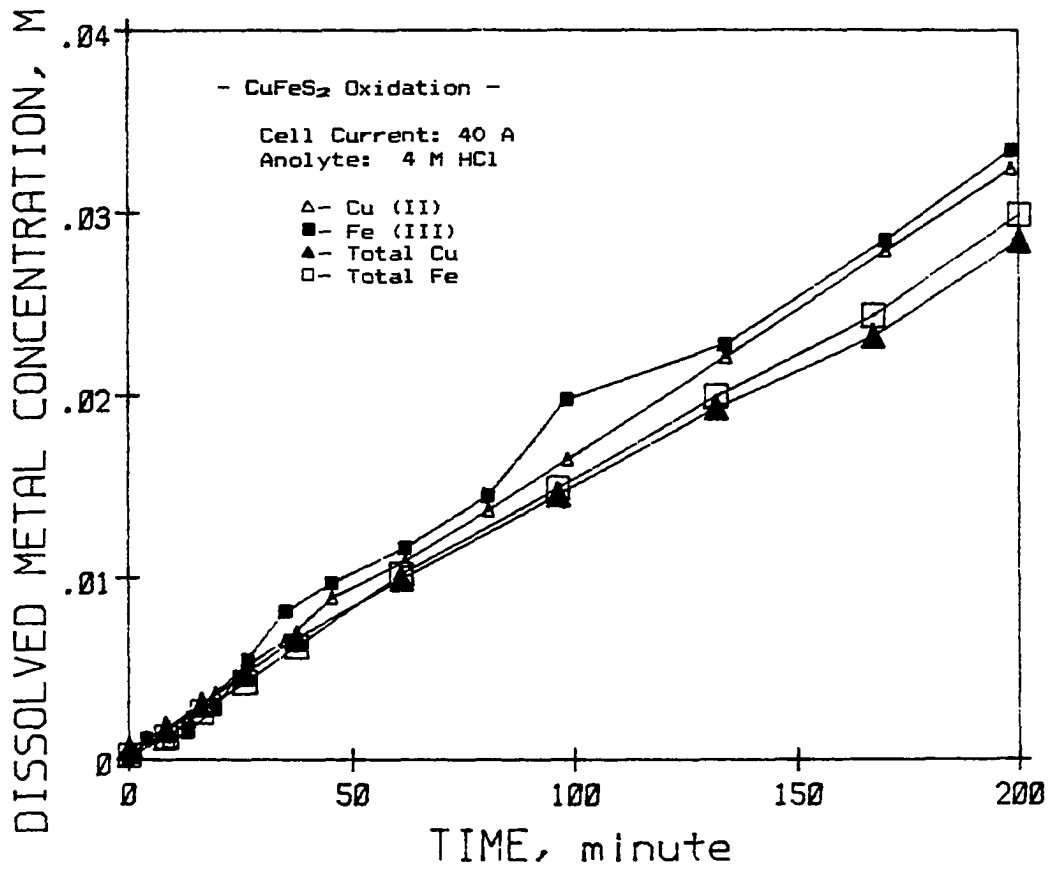

Figure 27. Total Cu and Fe, and the Cu (II) and Fe (III) concentrations during the anodic dissolution of $CuFeS_2$ in 4 M HCl

The oxidation of FeS_2 in 4 M HCl was also investigated. In Figure 28 are the scanning electron micrographs of the product resulting from the anodic dissolution of FeS_2 in 4 M HCl. The FeS_2 micrographs show no evidence of any elemental sulfur formation. The sulfur was instead oxidized to SO_4^{2-}. Based on the stoichiometry of reaction (60), the current efficiency for the oxidation of FeS_2 was calculated to be greater than 95 % at all times. A small amount of Cl_2 evolution was detected by olfactory inspection of the electrolyte samples.

$$FeS_2 + 8\ H_2O \longrightarrow Fe^{3+} + 2\ SO_4^{=} + 16\ H^+ + 15\ e^- \qquad (60)$$

The oxidation of $Cu_{1.8}S/FeS_2$ mixtures in 4M HCl was found to produce no Cu (I). The absence of Cu (I) would be expected, since the oxidation of FeS_2 would produce Fe (III), which after reacting with Cu (I) could be reoxidized at the electrode surface, thus providing an efficient mechanism for the elimination of Cu (I) as soon as it is produced.

The effect of the anolyte temperature on the rate of oxidation of $Cu_{1.8}S$ can be seen in Figure 29. There was essentially no temperature effect on the rate of dissolution until the solid phase composition reached approximately CuS. At that point, increasing the temperature caused the rate of CuS dissolution to increase. The increased rate of CuS dissolution with temperature could have been due to an increase in the rate of oxidation by Cl_2. This explanation seems plausible since the dissolution of copper sulfides by Cl_2 has been shown to increase with temperature [17]. The data for the dissolved Cu concentration in

Figure 28. Scanning electron micrographs of oxidized $CuFeS_2$ and FeS_2

100 μm

Sulfur Layer

40 μm

FeS_2 Surface

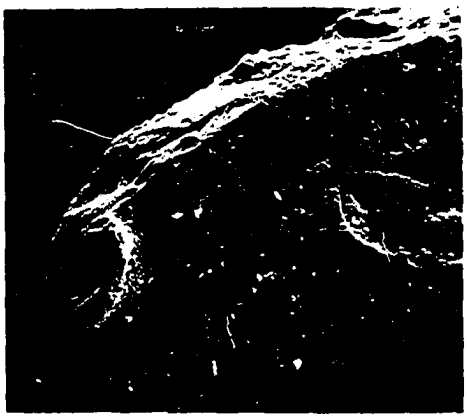

500 μm

Oxidized $CuFeS_2$ Particle

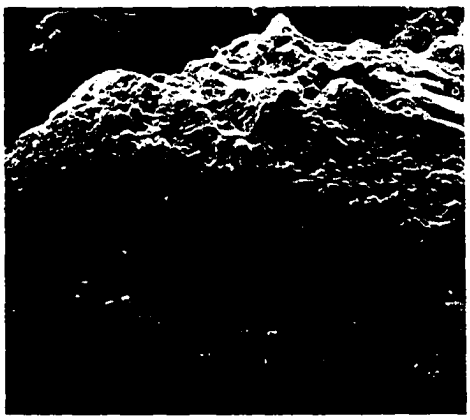

500 μm

Oxidized FeS_2 Particle

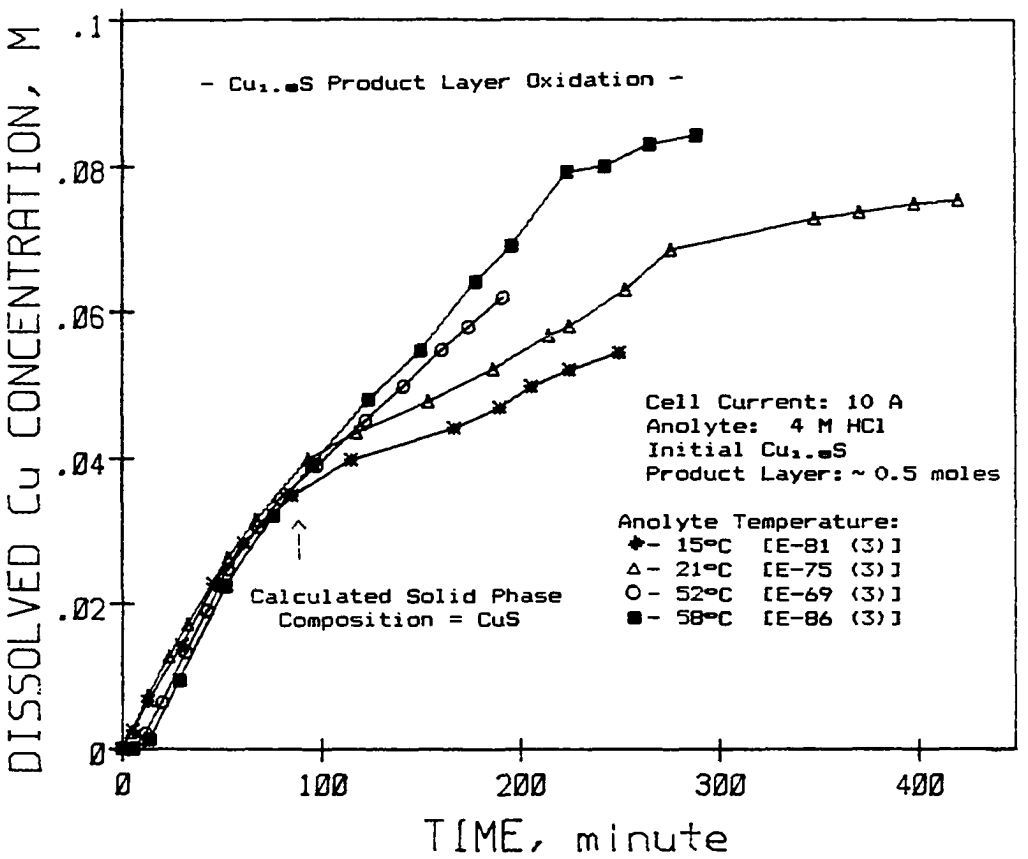

Figure 29. Dependence of the rate of oxidation of the $CuFeS_2$ reduction product layer on the electrolyte temperature

Figure 29 were corrected in order to account for the dissolution of $CuFeS_2$. That way the data represent only the rate of copper sulfide dissolution. (The data were corrected by assuming that the molar quantity of dissolved Cu that was produced from the dissolution of $CuFeS_2$ was equal to the molar amount of Fe produced.)

Shown in Figure 30, are the current efficiency versus time data for the oxidation of the $Cu_{1.8}S$ product layer in 4 M HCl, at various cell currents. As the cell current was increased from 19.5 to 28.5 amps, the amount of Cu (I) produced decreased (as indicated by the decrease in the current efficiency). But even when the cell current was as high as 53 amps, the current efficiency remained above 100% (based on the production of Cu^{2+}) until the metal phase stoichiometry reached CuS. At that point, Cl_2 evolution began and the current efficiency dropped steadily with the fraction of $Cu_{1.8}S$ reacted. The drop in current efficiency with increasing cell current, shown in Figure 30, was probably due to the oxidation of Cu (I) by the higher electrode potential that would have accompanied the increase in the cell current.

In Figure 31, the data are shown for the dissolution of the $Cu_{1.8}S$ product layer as a function of the initial $CuFeS_2$ particle radius. The initial $CuFeS_2$ particle radius had very little, if any effect at all on the rate of oxidation of the $Cu_{1.8}S$ product layer. An effect due to the size of the original particles would have been observed if the oxidation of $Cu_{1.8}S$ had been mass transfer controlled. The oxidation of $Cu_{1.8}S$ was not mass transfer controlled by the rate of diffusion of reactants through

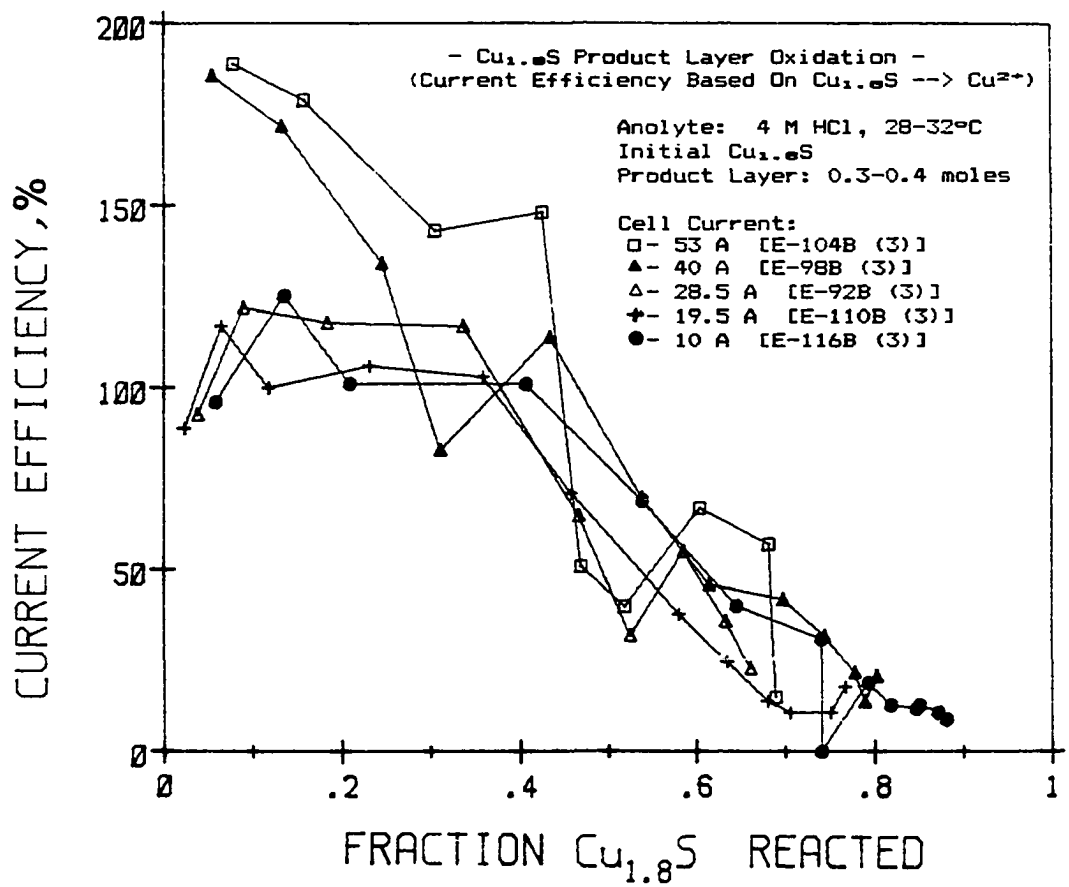

Figure 30. Dependence of the current efficiency on the fraction of the $CuFeS_2$ reacted as a function of the total cell current (Current efficiency was calculated assuming Cu^{2+} was the only dissolution product)

the product layer, because there were no reactants other than the $Cu_{1.8}S$ (excluding the possibility of Cl_2 dissolution mechanism). The only other type of mass transfer control would have been due to the mass transfer limited diffusion of the dissolved Cu species from the reacted surface, through the product layer, to the bulk solution. A build up of dissolved Cu at the reacting surface could have caused the rate of $Cu_{1.8}S$ to decrease because of concentration polarization. However, that would not be very likely since (i) the product layer porosity was large to begin with, (ii) the product layer porosity increased with Cu dissolution and (iii) the product layer thickness did not increase with Cu dissolution.

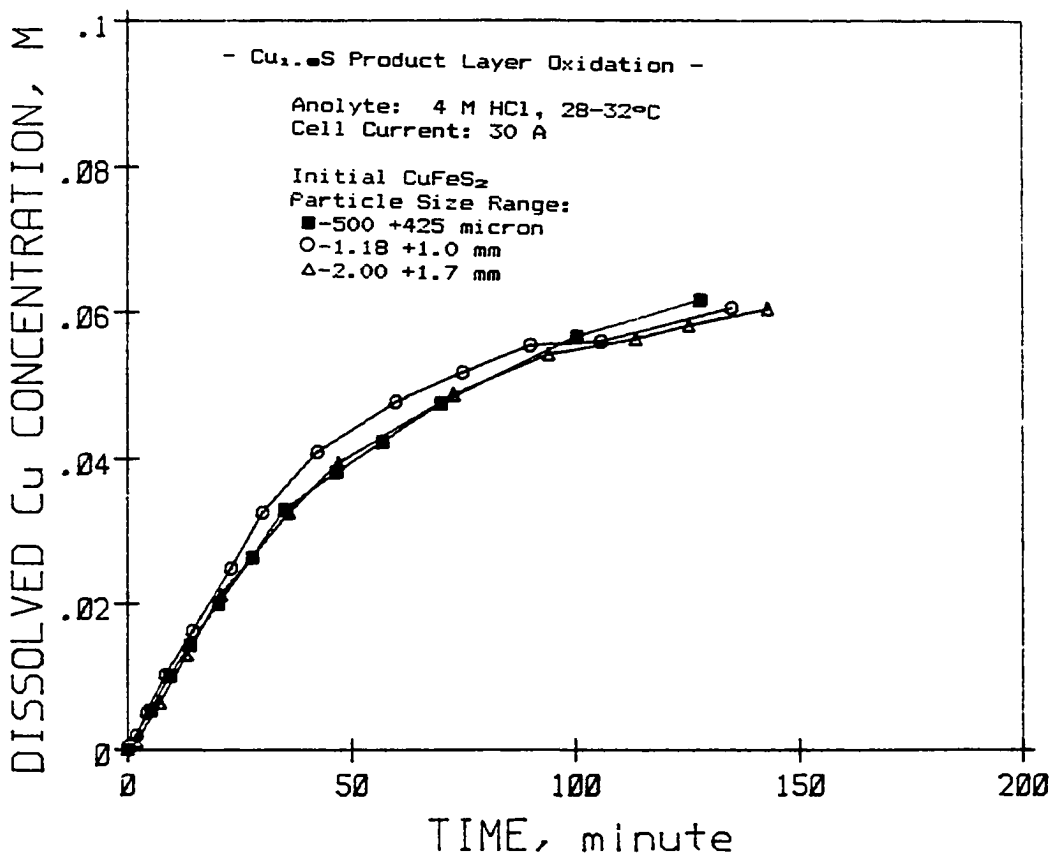

Figure 31. Dependence of the rate of $Cu_{1.8}$ dissolution on the initial $CuFeS_2$ particle size range

VI. CONCLUSION

A novel 2 stage process for the separation and recovery of the Cu, Fe and S from chalcopyrite was investigated. In stage 1, $CuFeS_2$ particles were reduced in the catholyte chamber of a fluidized bed electrochemical reactor. A digenite product layer formed on the unreacted $CuFeS_2$ and Fe (II) dissolved into the catholyte solution. Essentially, all of the Cu remained in the solid phase. In stage 2, the chalcopyrite reduction product layer from stage 1 was oxidized in an electrolyte different from that used in stage 1. The final products of stage 2 were Cu (I), Cu (II) and S^o. The overall process resulted in the dissolution and separation the Cu and Fe in $CuFeS_2$ into an Fe rich electrolyte and a Cu rich electrolyte. The S in $CuFeS_2$ reacted to form H_2S and S^o.

A mathematical model was developed to explain the chalcopyrite reduction results. The major assumptions in developing the model were (i) the rates of $CuFeS_2$ reduction and H_2 evolution were functions of the H^+ concentration at the reaction surface and (ii) the H^+ concentration at the reacting surface was limited by H^+ diffusion through the porous $Cu_{1.8}S$ product layer. Two constants were calculated from the experimental data in order to correlate the model with the investigative results.

The rate constant used in the model, K, was calculated by extrapolating to t=0, the fractional current data for the reduction of $CuFeS_2$. K was found to be a function of the electrolyte composition. The second constant, D_{H+} was determined by fitting the model with the K value to one set of experimental data.

The model was found to be in general agreement with the experimental data over a wide range of conditions. The model agreement indicates that the reduction of $CuFeS_2$ is controlled by the diffusion of H^+ through the porous product layer.

The reduction of chalcopyrite was severely inhibited by the formation of the reduction product layer. Model predictions indicated that it would be impossible to react the major portion of $CuFeS_2$ unless the product layer was removed, or a very low cell current was used. Experimentally, this was also found to be the case. Product layer removal in an ultrasonic bath was found to produce a product layer material that contained up 15 times more Cu than Fe. Successful operation of the proposed two stage electrodissolution process would most likely require the continuous removal of the chalcopyrite reduction product layer as it was formed.

Using AES and EDXS, the chalcopyrite reduction product which formed in 4 M HCl, was determined to be digenite. The AES and EDXS experiments, designed to determine the product layer composition that resulted from the electroreduction of $CuFeS_2$ in 4 M $HClO_4$, 2 M H_2SO_4 and 2.7 M H_3PO_4, were not precise enough to determine if the product layer was $Cu_{1.8}S$ or Cu_2S.

The experimental results indicated that the rate of reduction of $CuFeS_2$ in 4 M HCl was insensitive to the electrolyte temperature over the range of 15–58 ^oC. This was interpreted as being an indication that the activation energies for the reduction of chalcopyrite and the evolution of hydrogen on a chalcopyrite surface were similar.

Cu (I) was the major dissolution product resulting from the

electrochemical oxidation of natural chalcocite in 4 M HCl.

Oxidation of the chalcopyrite reduction product layer in 4 M HCl was found to produce Cu (I) until the copper sulfide composition reached CuS. At that point, the only copper dissolution species was Cu (II). This was a result of the increased electrode potential, caused by the rise in the rest potential of the copper sulfide as Cu was removed. In 4 M HCl, the amount of Cu (I) that was produced fell sharply when the total cell current exceeded 19.5 amperes. The higher electrode potential, at a higher applied currents, caused the rate of Cu (I) oxidation to increase.

Oxidation of the chalcopyrite reduction product layer was also possible in 4 M $HClO_4$, 2 M H_2SO_4 and 2.7 M H_3PO_4, except that Cu (II) was the only dissolution product, and O_2 evolution was the main reaction occurring after the copper sulfide stoichiometry reached CuS. Addition of Cl^- to the electrolyte prevented the production of O_2 and caused the CuS to react to Cu (II) and S^o. The presence of Cl^- also caused the evolution Cl_2.

In all of the oxidation experiments, the dissolution of CuS to Cu (II) and S^o was accompanied by Cl_2 evolution.

The sulfur layer that formed during the oxidation of the CuS product layer, was porous enough that the complete oxidation of the chalcopyrite reduction product layer was possible.

FeS_2 contamination of the $CuFeS_2$ prevented the formation of Cu (I) during the oxidation of the chalcopyrite reduction product layer. This was because the dissolution product of FeS_2 oxidation, Fe (III), oxidized the Cu (I). FeS_2 was also found to have a negative effect on the

reduction of $CuFeS_2$ because of its low overpotential for H_2 evolution. Successful operation of the proposed two stage electrochemical dissolution process would require the removal of the FeS_2 before reducing the $CuFeS_2$.

VII. RECOMMENDATIONS FOR FUTURE WORK

Based on the accumulated experimental results described above, $CuFeS_2$ froth flotation concentrate would be a good test material for future work involved in the investigation of the proposed 2 stage process. A froth flotation copper concentrate is comprised of smaller particles that those tested in this study. Diffusion limitations would not be as great. The concentrate would also contain very little FeS_2, making it possible to recover Cu (I) during the oxidation stage.

If copper concentrate from a froth flotation cell were used as a starting material, very low electrolyte flow rates would be required in order to prevent the particles from being swept out of the reactor. In this case a packed bed reactor would be a better choice for a reactor than a fluidized bed reactor.

Future experimental work should also concentrate on the determining the optimum electrolyte conditions for the proposed process. The results of this study indicate that both HCl and $HClO_4$ give comparable results for the reduction stage. Based on the results of the oxidation experiments alone, the better electrolyte choice would be HCl, because it allows Cu (I) to be formed. Using HCl for both the reduction and oxidation stages would simplify the process and might even make it economically more feasible. Using one electrolyte instead of two would have the advantage of requiring a smaller acid inventory. HCl also poses less material handling problems than does $HClO_4$.

Conditions which result in the least adherent product layer should

also be investigated. Although the nonadherency of the product layer was considered a problem in this study, a nonadherent $Cu_{1.8}S$ product layer might actually be desired if larger chalcopyrite particles were reacted, because the product layer prevents the complete reaction of the chalcopyrite. Removing the product layer with the circulating electrolyte, and collecting it somewhere else would prevent the diffusion of H^+ from controlling the process. By removing the product layer and reacting it in another location, the process could be made continuous.

An investigation into the mechanism for the electrooxidation of CuS and $CuFeS_2$ is also advised. Experiments need to be performed to determine if CuS and $CuFeS_2$ were chemically oxidized by Cl_2, Fe (III) or Cu (II), or if they reacted electrochemically. Measuring the solid phase resistance of the sulfur coated oxidation products would indicate if particle-particle charge transfer is possible. If the solid phase resistance turns out to be very high, it would indicate that CuS and $CuFeS_2$ are chemically oxidized by the Cl_2, Fe (III) or Cu (II). Further experiments could then be performed to determine which oxidant is most selective for the dissolution of CuS. The oxidant could then be produced as efficiently as possible and circulated through a reactor filled with the CuS product.

VIII. REFERENCES

1. Backhurst, J. R., J. M. Coulsom, F. Goodridge and R. E. Plimley. 1969. A preliminary investigation of fluidized bed electrodes. J. Electrochem. Soc. 116:1600-1607.

2. Bareau, J. Y. and F. Coeuret. 1979. The anodic dissolution of copper in a fluidized bed electrode. J. Appl. Electrochem. 9:737-743.

3. Bautista, R. G. and D. S. Flett. 1976. Electrodissolution in hydrometallurgy. Warren Spring Laboratory Report, No. LR 226 (ME).

4. Bertram, R., E. Hillrichs, N. Galitas, R. Muller and H. Greulich. 1981. Electrochemical leaching of copper sulphide ores. Dev. Miner. Process., A. 2:810-824.

5. Bertram, R., E. Hillrichs and R. Muller. 1983. Anodic dissolution of copper sulphide ores in molten $ZnCl_2$-KCl. Trans. Inst. Mining Metall. 92:C169-C171.

6. Biegler, T. and D. C. Constable. 1976. Upgrading and activation of chalcopyrite concentrates by slurry electrolysis. Trans. Inst. Mining Metall. 85:C23-C29.

7. Biegler, T. and D. C. Constable. 1977. Continuous electrolytic reduction of a chalcopyrite slurry. J. Appl. Electrochem. 7:175-179.

8. Biegler, T. and D. A. Swift. 1976. The electrolytic reduction of chalcopyrite in acid solution. J. Appl. Electrochem. 6:229-235.

9. Biegler, T. and D. A. Swift. 1976/1977. Dissolution kinetics of copper sulfide anodes. Hydrometallurgy 2:335-349.

10. Biegler, T. and D. A. Swift. 1979. Anodic electrochemistry of chalcopyrite. J. Appl. Electrochem. 9:545-554.

11. Biegler, T. and D. A. Swift. 1979. Anodic behavior of pyrite in acid solutions. Electrochim. Acta 24:415-420.

12. Brennet, P., S. Jafferali, J. Vanseveren, J. Vereeken and R. Winand. 1974. Study of the mechanism of anodic dissolution of Cu2S. Met. Trans. 5 (1):127-134.

13. Cavallotti, P. and G. Salvago. 1969. Electrodic behavior of copper sulphides in aqueous solutions. Electrochim. Metal. 4 (3):181-210.

14. Coeuret, F. 1980. The fluidized bed electrode for the continuous recovery of metals. J. Appl. Electrochem. 10:687-696.

15. Coeuret, F., P. Le Goff and F. Vergnes. 1967. Particulate electrode system. French Patent No. 1,500,269.

16. Das, S. C. 1978. Fluidized bed electrode; a novel technique in extractive metallurgy. J. Electrochem. Soc. India 27:235-240.

17. Etienne, A. 1970. Electrochemical aspects of the aqueous oxidation of copper sulphides. Ph.D Thesis, Univ. of British Columbia.

18. Fahidy, T. Z. 1973. The chemical engineering approach to some electrochemical processes. Can. J. Chem. Eng. 51:521-535.

19. Fleischmann, M., F. Goodridge, J. R. Backhurst, and R. E. Plimley. 1976. Fluidized electrodes for producing metanilic acid electrochemically. British Patent No. 1,194,181.

20. Fleischmann, M. and J. W. Oldfield. 1971. Fluidized bed electrodes. Part I. Polarization predicted by simplified models. J. Electroanal. Chem. 29:211-230.

21. Fleischmann, M. and J. W. Oldfield. 1971b. Fluidized bed electrodes. Part II. The effective resistivity of the discontinuous metal phase. J. Electroanal. Chem. 29:231-240.

22. Fleischmann, M., J. W. Oldfield and D. F. Porter. 1971. Fluidized bed electrodes. Part III. The cathodic reduction of oxygen on silver in a fluidized bed electrode. J. Electroanal. Chem. 29:247-253.

23. Fleischmann, M., J. W. Oldfield and L. Tennakoon. 1971. Fluidized bed electrodes. Part IV. Electrodeposition of copper in a fluidized bed of copper-coated spheres. J. Electroanal. Chem. 29:103-112.

24. Garrels, R. M. and C. L. Christ. 1965. Figure 7.24. Pg. 232 in Solutions, minerals and equilibria. Harper and Row, New York.

25. Gerlach, J. and E. Kuzeci. 1983. Application of carbon paste electrodes to elucidate hydrometallurgical dissolution processes with special regard to chalcocite and covellite. Hydrometallurgy 11:345-361.

26. Ghali, E. and A. Lewenstam. 1982. Electrodissolution of synthetic covellite in hydrochloric acid. J. Appl. Electrochem. 12:369-376.

27. Goodridge, F. 1968. Design of continuous electrolytic cells. Chem. and Proc. Eng. 49:93-95, 100.

28. Goodridge, F., D. I. Holden, H. D. Murray and R. F. Plimley. 1971. Fluidized bed electrodes. Part I. A mathematical model of the fluidized bed electrode. Trans. Instn. Chem. Engrs. 49:128-136.

29. Habashi, F. and N. Torres-Acuna. 1968. The anodic dissolution of copper(1) sulfide and the direct recovery of copper and elemental sulfur from white metal. Trans. Met. Soc. AIME 242 (5):780-787.

30. Hangovan, S., D. R. Nagaraj and K. I. Vassu. 1975. Electrometallurgy of chalcopyrites-II: copper powder from slurry anodes. J. Electrochem. Soc. India 24 (4):195-199.

31. Hepal, M. and T. Hepal. 1977. The anodic dissolution of chalcocite in an ammoniacal environment. J. Electroanal. Chem. 81:161-170.

32. Hillrichs, E. and R. Bertram. 1983. Anodic dissolution of copper sulphides in sulfuric acid solution. II. The anodic decomposition of CuS. Hydrometallurgy 11:195-206.

33. Hillrichs, E., H. Greulich and R. Bertram. 1983. Investigation of the electrochemical dissolution of copper sulfide ores in sulfuric acid solutions. Pp. 277-287 in K. Osseo-Assare and J. D. Miller, eds. Hydrometallurgy Research, Development and Plant Practice. American Institute of Mining, Metallurgical and Petroleum Engineers, Inc., New York.

34. Hojo, M. and E. Peters. 1981. Direct electrorefining of chalcocite. J. Electroanal. Chem. 118:345-364.

35. Kimura, R. T., P. A. Haunschild and K. C. Liddell. 1984. A mathematical model for calculation of equilibrium solution speciations for $FeCl_3$-$FeCl_2$-$CuCl_2$-CuCl-HCl-NaCl-H_2O system at 25°C. Metall. Trans. 15B:213-219.

36. Kuxmann, U. and H. Biallass. 1969. Zur anodischen auflosung von chalcopyrit. Erzmetall 22 (2):53-64.

37. Le Goff, P., F. Vergnes, F. Coeuret and J. Bordet. 1969. Applications of fluidized beds in electrochemistry. Ind. Eng. Chem. 61:8-17.

38. Mackinnon, D. J. 1976. Fluidised-bed anodic dissolution of chalcocite. Hydrometallurgy 1:241-257.

39. Mackinnon, D. J. 1976. Fluidised-bed anodic dissolution of covellite. Hydrometallurgy 2:65-76.

40. Marchese, E. 1882. German Patent 22,429.

41. McMillan, R. S., D. J. MacKinnon and J. E. Dutrizac. 1982. Anodic dissolution of n-type and p-type chalcopyrite. J. Appl. Electrochem. 12:743-757.

42. Mehendale, S. G., S. Venkatachalam and R. Mallikarjunan. 1982. Studies on the anodic dissolution of copper matte. Hydrometallurgy 9:195-204.

43. Newman, J. S. and C. W. Tobias. 1962. Theoretical analysis of current distribution in porous electrodes. J. Electrochem. Soc. 109:1183-1191.

44. Parker, A. J., R. L. Paul and G. P. Power. 1981. Electrochemistry of the oxidative leaching of copper from chalcopyrite. J. Electroanal. Chem. 118:305-316.

45. Peters, E. 1977. The electrochemistry of sulfide minerals. Pp. 267-290 in J. Bockris, D. A. J. Rand and B. J. Welch eds. Proc. 4th Aust. Electrochem. Conf.,1976. Plenum Press, New York.

46. Peters, E. and H. Majima. 1972. Electrochemical reactions of pyrite in acid perchlorate solutions. Can. Metall. Quart. 7 (3):111-117.

47. Price, D. C. 1981. Application of chronopotentiometric analysis to the anodic treatment of copper sulphides. Met. Trans. B 12B (6):231-239.

48. Price, D. C. and J. P. Chilton. 1980. The electroleaching of bornite and chalcopyrite. Hydrometallurgy 5:381-394.

49. Price, D. C. and J. P. Chilton. 1981. The anodic reactions of bornite in sulfuric acid solution. Hydrometallurgy 7:117-133.

50. Sabacky, B. J. and J. W. Evans. 1977. The electrical conductivity of fluidized bed electrodes - its significance and some experimental measurements. Metal. Trans. B 8b:5-13.

51. Sabacky, B. J. and J. W. Evans. 1979. Electrodeposition of metals in fluidized bed electrodes. Part I. Mathematical model. J. Electrochem. Soc. 7:1176-1180.

52. Thangappan, R. and H. V. K. Udupa. 1974. Fluidized-bed electrodes - A review. Trans. Soc. Adv. Electrochem. Sci. Technol. 9:59-63.

53. Vargas, T. and D. Inman. 1981. The anodic dissolution of chalcopyrite in water + acetonitrile solutions. J. Electroanal. Chem. 119:25-40.

54. Venkatachalam, S. and R. Mallikarjunan. 1968. Direct electrorefining of cuprous sulphide and copper matte. Trans. Inst. Min. Metall. 77:C45-C52.

55. Venkatachalam, S. and R. Mallikarjunan. 1971. Laboratory scale studies on a new procedure for the recovery of electrolytic copper. Trans. Ind. Inst. Met. 24 (2):29-38.

56. Warren, G. W., M. E. Wadsworth and S. M. El-Raghy. 1982. Anodic behavior of chalcopyrite in sulfuric acid. Pp. 261-275 in K. Osseo-Assare and J. D. Miller, eds. Hydrometallurgy Research, Development and Plant Practice. American Institute of Mining, Metallurgical and Petroleum Engineers, Inc., New York.

IX. ACKNOWLEDGMENTS

The author wishes to thank Dr. Renato G. Bautista for his help and guidance during the course of this study. The other members of the advisory committee are thanked for their interest and helpful suggestions, especially Dr. Dennis Johnson.

Mr. Harvey Jensen is thanked for his invaluable assistance in constructing and maintaining all of the experimental equipment and for his culinary expertise.

My friends and fellow graduate students are thanked for making life in Ames a convivial time; especially Angel, Ahkmeed, Bergie, Herb, HP, King, Kevo and Zoro.

I would also like to acknowledge the financial support in the form of a graduate assistantship from the Iowa State University Mining and Minerals Resources Research Institute for the first year of this degree program and the graduate assistantship for the balance of the degree program from the United States Department of Energy, Office of Basic Energy Sciences, Chemical Sciences Program, WPAS-KC-03-02-02.

X. APPENDIX

A list of the major pieces of equipment used during the course of this study and the address for obtaining a copy of the experimental data are given in this section.

A. List of Experimental Equipment

Table 7. List of experimental equipment

Equipment Make and Model	Function
Perkin Elmer Atomic Absorption Spectrophotometer Model 5000	Measure total dissolved metal ion concentrations
Perkin Elmer Scanning Auger Electron Microprobe Model 600	Measure surface concentrations of Cu, Fe and S
TN Energy Dispersion X-ray Spectrophotometer Model 600	Measure surface concentrations of Cu, Fe and S
Sorensen DC Power Supply Model DCR10-170B	Provide direct current to FBER
Apple IIe Computer and IMI Data Acquisition System	Data acquisition and calculations

B. Experimental Data

The data that were collected during the course of this study are too voluminous to be included in this dissertation. If a copy of the data is required, it can be obtained by sending a written request to:

Ames Laboratory Document Library

201 Spedding Hall

Iowa State University

Ames, Iowa 50011